Chemical Geology 500 (2018) 159–174

Contents lists available at ScienceDirect

Chemical Geology

journal homepage: www.elsevier.com/locate/chemgeo

Chemical weathering of small catchments on the Southeastern Tibetan Plateau I: Water sources, solute sources and weathering rates

Hao Jiang[a,b,c,d], Wenjing Liu[a,b,c,d,*], Zhifang Xu[a,b,c,d,*], Xiaode Zhou[a,b,c,d], Ziyan Zheng[d,e], Tong Zhao[a,b,c,d], Li Zhou[f], Xuan Zhang[a,b,c,d], Yifu Xu[a,b,c,d], Taoze Liu[g]

[a] Key Laboratory of Cenozoic Geology and Environment, Institute of Geology and Geophysics, Chinese Academy of Sciences, Beijing 100029, China
[b] CAS Center for Excellence in Life and Paleoenvironment, Beijing 100044, China
[c] Institutions of Earth Sciences, Chinese Academy of Sciences, Beijing 100029, China
[d] University of Chinese Academy of Sciences, Beijing 100049, China
[e] Key Laboratory of Regional Climatic-environment for Temperate East Asia, Institute of Atmospheric Physics, Chinese Academy of Sciences, Beijing 100029, China
[f] State Key Laboratory of Biogeology and Environmental Geology, China University of Geosciences, Wuhan 430074, China
[g] State Key Laboratory of Environmental Geochemistry, Institute of Geochemistry, Chinese Academy of Sciences, Guiyang 550081, China

ARTICLE INFO

Editor: Jerome G.

Keywords:
Small catchment
Chemical weathering
Solute sources
Tibetan Plateau

ABSTRACT

Hydro-geochemical study of small catchment provides important information to identify water and solute sources, understand chemical weathering processes and their controlling factors. In this work, 44 small catchments on the southeastern Tibetan Plateau were investigated. Stream, precipitation, glacier and spring waters in both high and low flow seasons and bed rocks samples were analyzed with a main purpose to understand the processes controlling the stream water chemistry and quantify the weathering rates. The stream waters are mainly recharged by precipitation and glacier meltwater. Glacier meltwater and precipitation account for 25.8% and 73.9% of the total discharge in high flow season, and 44.4% and 54.1% in low flow season on average. Hydrograph separation and chemical mass balance are jointly used to estimate the contributions of major reservoirs (precipitation, glacier, spring, carbonates and silicates) to the total dissolved loads of the streams. Rock weathering accounts for ~90% of the total dissolved cations for most streams. Silicate and carbonate weathering account for 15.9% and 75.2% of total dissolved cations in high flow season, and 9.5% and 77.2% in low flow season on average. Lack of basic hydrological data in the ungauged remote area is a problem for quantified weathering study. The Noah LSM model is applied to obtain the annual runoff of these un-gauged catchments in this study. Based on these approaches, the chemical weathering rates and total denudation rates (TDR) are calculated for each of the small catchments. The silicate cation weathering rates (SCWR) range between 0.6 and 5.2 t/km^2/yr, with the area-weighted mean value about 1.8 t/km^2/yr. The TDR range between 8.9 and 1907.9 t/km^2/yr. The comparisons between the small catchments and with other river basins in different tectonic and climatic environments indicate that lithology, climatic factors (temperature and runoff) and physical erosion rate are the key parameters controlling chemical weathering rate. The average SCWR of the small catchments is about 6 times higher in high flow season than in low flow season, which could be attributed to the higher temperature and runoff in high flow season. Meanwhile, the positive relationship between SCWR and TDR supports the view that physical erosion has an important effect on chemical weathering in the Tibetan Plateau.

1. Introduction

Rock weathering is one of the most important processes that control the evolution of the Earth's surface and regulate global element cycling (Berner et al., 1983; Kasting, 1987; Berner, 1991; Louvat and Allègre, 1997; Gaillardet and Galy, 2008). Silicate weathering is thought to control global climate over geological time scales through atmospheric CO_2 consumption (Walker et al., 1981; Berner, 1991). Many studies have used chemical fluxes of rivers to estimate chemical weathering and associated CO_2 consumption rates at basin and continental scales (e.g., Gaillardet et al., 1997, 1999; Krishnaswami et al., 1999; Jacobson et al., 2002; Dalai et al., 2002; Huh, 2003; Singh et al., 2005; Tipper

* Corresponding authors at: Key Laboratory of Cenozoic Geology and Environment, Institute of Geology and Geophysics, Chinese Academy of Sciences, Beijing 100029, China.
E-mail addresses: liuwenjing@mail.iggcas.ac.cn (W. Liu), zfxu@mail.iggcas.ac.cn (Z. Xu).

https://doi.org/10.1016/j.chemgeo.2018.09.030
Received 29 December 2017; Received in revised form 19 September 2018; Accepted 22 September 2018
Available online 01 October 2018
0009-2541/

et al., 2006; Qin et al., 2006; Chetelat et al., 2008; Moon et al., 2014; Wang et al., 2016; Das et al., 2016; Li et al., 2018). Rivers originating from the Tibetan Plateau have drawn extensive attention due to the potential impact of tectonic uplift on chemical weathering and carbon dioxide cycling and global climate changes (Raymo et al., 1988; Raymo and Ruddiman, 1992; Ruddiman, 1997). According to the previous studies, a rough trend in silicate weathering rates in the Tibetan Plateau was found in the order of northern < western < eastern < southern (Galy and France-Lanord, 1999; Gaillardet et al., 1999; Wu et al., 2005, 2008; Wu, 2016; Hren et al., 2007; Moon et al., 2007; Noh et al., 2009; Li et al., 2014a). However, quantitative understanding of the chemical weathering as well as its controlling factors in the Tibetan Plateau remain challenges because of complex lithologies, imprecise end-members, interfere of anthropogenic activities and various climatic and tectonic zones in large basin scales. In contrast, weathering studies at small catchment scale have been well documented to provide information on end-member identification, solute origin, weathering rate and the controlling factors (e.g., lithology, climate, topography, biological and anthropogenic activities), which can be simplified to the most extent at small catchment scale (White and Blum, 1995; Millot et al., 2002; West et al., 2002, 2005; Oliva et al., 2003; Meyer et al., 2009; Fernandes et al., 2016). Moreover, the research on chemical dynamics of weathering and its controlling factors in small catchments can be helpful in understanding the integrated processes, as well as accurately estimating the chemical weathering and associated CO_2 consumption rates of large river basins. However, at present there is a lack of studies for small simple lithology catchments on Tibetan Plateau, compared with large river basin studies there.

Small catchments are generally located at the river head in mountainous areas. Identifying the solute sources is challenging, because various reservoirs (e.g., glacier, precipitation, hot spring and various rocks weathering) may contribute to dissolved loads of streams (Louvat and Allègre, 1997; Hagedorn and Whittier, 2015). The combined use of hydrological approach (hydrograph separation, Buttle, 1994; Zhou et al., 2015) and geochemical approach (mass balance, Garrels and Mackenzie, 1967) could shed lights on this problem, which provides a new perspective to understand the processes controlling stream water chemistry and improves the quantification of weathering rates (Hindshaw et al., 2011). Here we carry out hydro-geochemical investigation of 44 small catchments on the southeastern Tibetan Plateau. The main purpose of this paper is to discuss the hydro-geochemical processes controlling the water geochemistry, quantify the contributions of the different sources to the dissolved loads and calculate the chemical weathering rates. In addition, the controlling factors of chemical weathering in the mountainous plateau background are explored through the comparisons between the small catchments and with other river basins in different tectonic and climatic environments.

2. Geological and geographical settings

The 44 small catchments in this study are located on the eastern slope of the Mount Gongga, southeastern Tibetan plateau (Fig. 1). The small catchments are sub-catchments of four river basins, which are the Jiazela River basin (JR), Yajia River basin (YR), Dadu River basin (DR), and Nanya River basin (NR). The catchments areas range from 0.56 km^2 to 46 km^2, and the elevations range from 1000 m to 3400 m (sample sites).

The geographical parameters and geological information of the small catchments are listed in Table 1. Proterozoic granitoids (mainly granite, biotite granite, plagiogranite and diorite) are widely exposed in the study area. Most of the small catchments are underlined by granitic lithologies, except for those on the west bank of the Yajia River (WY), where metamorphic rocks (mainly schist, slate, crystalline limestone and marble) of late Paleozoic age are exposed (Fig. 1). The granitoids of the small catchments of JR and WY are mainly biotite granites. The lithologies of the east bank of the Yajia River (EY) are mainly plagiogranites. The granitoids of DR and NR are mainly granites. Besides, diorites, with amphibole contents of 40–55% (Geological Bureau of Sichuan Province, 1974a, 1974b), are distributed in this region. The descriptions of the rocks are provided in Table 4. Quaternary sedimentary rocks, mostly consisting of siliciclastic rocks, gravel rocks and clays, are distributed on the stream beds of NR and YR. Carbonaceous shales and andesitic basalts are also distributed in this region. No stream drains such lithologies except for DR-4, which drains some shales. No salt-bearing stratum is observed in the studied area (Fig. 1) (Geological Bureau of Sichuan Province, 1974a, 1974b, 1977).

The climate of the catchments is characterized by the monsoon in high flow season and westerly circulation in low flow season (Li and Su, 1996). The mean annual air temperatures (MAT) during 2004–2014 observed at the Gongga Alpine Ecosystem Observation and Research Station (GAEOS) are 4.1 °C and 13.5 °C at the elevations of 3000 m and 1500 m, respectively. The mean annual precipitation (MAP) is 1900–1950 mm (Zhang et al., 2012; Wu et al., 2013; Zhou et al., 2016). Precipitation from May to October accounts for ~80% of the total annual precipitation (Zhang et al., 2012). Water discharge is highest during July to September and lowest during January to March. The discharge of May to October (high flow season) accounts for ~85% of the annual runoff according to the gauging stations of the GAEOS. Small catchments of DR and NR are characterized by soil-mantled and vegetated catchments, while those of JR and WY are mostly featured by barren bedrock and glaciers. Overall, the vegetation of low elevation regions (below 3200 m) is dominated by coniferous forest, and the vegetation is relatively sparse in high elevation regions, mainly composed of shrub. The studied streams flow through relatively pristine environments. There are little industrial or agricultural activities in the area. Hot springs are widely distributed in this region (Fig. 1).

3. Sampling and analytical methods

A total of 75 stream water samples, 11 precipitation samples, 12 hot spring samples, 3 glacial meltwater samples, 3 ground water samples and 21 fresh rock samples (2 schists and 19 granitoids) were collected from the small catchments in high flow season (July 2014) and low flow season (January 2015). The sampling locations are shown in Fig. 1. The elevations and coordinates of the sampling sites were recorded by GPS (GARMIN-RINO 650) with accuracy of 3–5 m. The drainage areas of the catchments were calculated by the geographical information system (GIS) software ESRI ArcGIS 10.3 using the shuttle radar topography mission (SRTM) digital elevation model (DEM). MAT of the sampling sites were estimated applying a homogeneous thermal gradient from the MAT observed by the GAEOS (White and Blum, 1995). The small catchments are in remote pristine mountainous areas, and only two of them have hydrological gauging stations (WY-1 and WY-13) (Li et al., 2004). To obtain the annual runoff of the un-gauged catchments, Noah land surface model (LSM) (Sellers et al., 1997; Pitman, 2003) offline version 3.3, which is forced by Princeton Meteorological datasets with horizontal resolution of 0.25°, was applied. The model is computationally efficient in precipitation-runoff simulations and was applied across the world in the context of small-scale and global-scale modeling (e.g., Niu et al., 2011; Yang et al., 2011; Xu et al., 2012).

Stream water samples were collected about 10 cm below the water surface at the confluences. Precipitation samples were collected for each precipitation event during the sampling period with a plastic cylinder at the GAEOS. Spring samples were collected at the outlets of the springs. After removal of the top few centimeters of the ice, the supraglacial samples were collected using a plastic ice scraper and packed into HDPE bottles and melted naturally. The ground water samples were outflowed waters collected on mountainsides. All the containers were previously washed with HCl and rinsed with pure-water (18.2 MΩ) and dried. The water samples were immediately filtered through 0.22 μm Millipore mixed cellulose esters membrane filters. The first portion of the filtrate was discarded to clean the membrane and

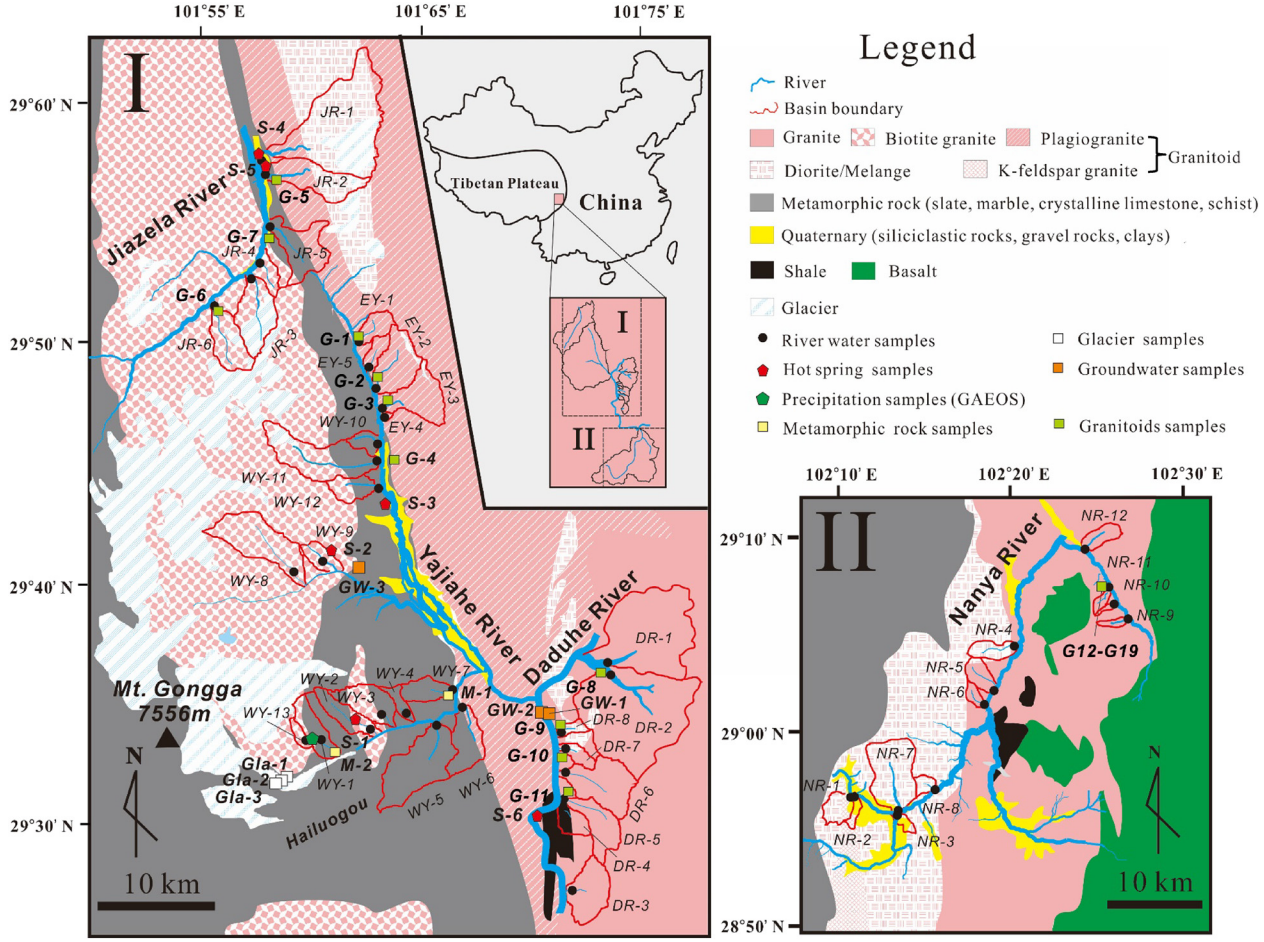

Fig. 1. Geological map and sample sites of the small catchments on the southeastern Tibetan Plateau. Area I contains the Jiazela river basin (JR), Yajia river basin (WY stands for west bank of Yajia River, EY stands for east bank of Yajia River) and Dadu river basin (DR), and area II represents Nanya River basin (NR), respectively. The geological information is derived from the 1:200000 geologic map (Geological Bureau of Sichuan Province, 1974a, 1974b, 1977).

containers. One aliquot is acidified with double sub-boiling distilled HNO_3 (6 M) to pH < 1.6 and stored in a polyethylene bottle for cations analysis and another is stored directly in a polyethylene bottle for anion analysis. The bedrock samples were collected at the stream beds across the entire region (Fig. 1).

The pH and electric conductance (EC) were measured in the field with a portable EC/pH meter (YSI-6920, USA). The HCO_3^- concentrations were titrated by hydrochloric acid within 12 h after sampling. The dissolved SiO_2 concentrations were determined by spectrophotometry with the molybdate blue method. Cations (K^+, Na^+, Ca^{2+} and Mg^{2+}) concentrations were analyzed using Inductively Coupled Plasma Atomic Emission Spectrometer (ICP-AES) (IRIS Intrepid II XSP, USA) with a precision of ± 3%, and anions (Cl^-, SO_4^{2-} and NO_3^-) concentrations were analyzed by ionic chromatography (Dionex 120, USA) with a precision of ± 5%. The suspended particulate matter (SPM) collected on the filters were removed in the clean laboratory using Millipore-Q water and the solution containing the SPM were dried at 55 °C. The solid residue was then weighed and the SPM contents were deduced (Chetelat et al., 2008). The water chemistry and SPM contents were conducted in the hydrochemistry and environmental laboratory at the Institute of Geology and Geophysics, Chinese Academy of Sciences (CAS). The δD and $\delta^{18}O$-H_2O were analyzed using Elemental Analyzer-Isotope Ratio Mass Spectrometer (EA-IRMS) at the State Key Laboratory of Atmospheric Boundary Layer Physics and Atmospheric Chemistry (LAPC), Institute of Atmospheric Physics, CAS. The isotopic data in this paper are reported in per mil (‰) relative to the ratios of the international VSMOW standard. Analytical uncertainties are ± 0.5‰ for δD and ± 0.1‰ for $\delta^{18}O$.

Analysis of the major-element of the bedrocks was carried out by wavelength dispersive X-ray fluorescence (WD-XRF) spectrometry at the ALS Minerals-ALS Chemex (Guangzhou) Co., Ltd. A calcined or ignited sample (0.9 g) was added to 9.0 g of Lithium Borate Flux (50%–50% $Li_2B_4O_7$-$LiBO_2$). They were mixed well and fused in an auto fluxer between 1050 and 1100 °C. A flat molten glass disc was prepared from the resulting melt. This disc was then analyzed by WD-XRF spectrometry with standard curve method. The standard samples were the national rock standard samples of China (GBW07101-07114 and GBW07295-07429). The uncertainties are < 5% for major-element oxides.

4. Results

4.1. Hydro-geochemistry of stream waters

The water quality parameters and chemical and isotopic compositions of the stream waters from the small catchments are presented in Table 2. The pH values of the stream waters are mostly mildly alkaline (6.9 to 8.9, averaging at 8.0). The total cation charge ($TZ^+ = Na^+ + K^+ + Ca^{2+} + Mg^{2+}$, in 10^{-6} charge equivalent units (μeq)) varies from 209 to 6676 μeq/l. The normalized inorganic charge balance ($NICB = 100 \times (TZ^+ - TZ^-)/TZ^+$) is generally within ± 10%, with an anionic deficit in most of the samples (Table 2), indicating an ionic equilibrium for the natural waters and that unanalyzed organic anions is only a minor component (Fernandes et al.,

Table 1
Geographic parameters and lithology of the small catchments on the southeastern Tibetan Plateau, China.

Sample	Longitude (E)	Latitude (N)	Elevation	MAT	Drainage area	Annual runoff[a]			Discharge[b]		Lithology[c]
			m	°C	km^2	mm/yr			l/s		
						H	L	annual	H	L	
Yajiahe River Basin											
WY-1	101°59′ 26.00″	29°34′ 22.80″	3038	3.9	1.5	498	88	586	108	0	B/M
WY-2	102°01′ 46.27″	29°35′ 21.00″	2583	6.7	7.5	607	107	714	444	8	B/M
WY-3	102°02′ 54.49″	29°35′ 41.83″	2272	8.7	9.1	444	78	523	839	40	B/M
WY-4	102°04′ 01.40″	29°36′ 10.71″	2062	10.0	3.5	375	66	441	77	23	M
WY-5	102°05′ 39.86″	29°36′ 20.84″	1816	11.5	19.1	444	78	523	1007	168	M
WY-6	102°06′ 42.24″	29°36′ 42.94″	1654	12.5	9.6	293	52	345	540	15	P/M
WY-7	102°06′ 12.49″	29°37′ 30.51″	1733	12.0	5.3	310	55	364	226	3	M
WY-8	101°59′ 51.71″	29°41′ 52.34″	2597	6.6	17.3	476	84	560	1540	2	B
WY-9	102°01′ 54.42″	29°42′ 13.91″	2273	8.7	4.1	404	71	475	299	63	B
WY-10	102°03′ 35.74″	29°46′ 55.14″	2462	7.5	3.1	357	63	420	357	38	M
WY-11	102°03′ 45.00″	29°46′ 36.15″	2408	7.8	19.6	826	146	972	2860	480	B/M
WY-12	102°03′ 31.73″	29°45′ 39.03″	2275	8.6	5.1	466	82	549	827	0	B/M
WY-13	102°00′ 15.08″	29°34′ 42.93″	2912	4.7	7.5	371	66	437	440	5	B
EY-1	102°02′ 21.39″	29°51′ 15.11″	3319	2.1	4.1	679	120	799	503	40	P
EY-2	102°03′ 22.18″	29°49′ 17.11″	2896	4.8	10.5	507	89	597	949	179	P
EY-3	102°03′ 39.67″	29°48′ 34.67″	2828	5.2	8.9	484	85	569	1425	206	P
EY-4	102°03′ 42.06″	29°48′ 21.89″	2801	5.3	1.6	435	77	511	57	0	P
EY-5	102°02′ 38.01″	29°50′ 08.98″	2990	4.2	3.0	528	93	621	242	5	P
Jiazela River basin											
JR-1	101°57′ 09.63″	29°58′ 46.06″	2912	4.7	16.0	1782	314	2097	2034	4	P/D/M
JR-2	101°57′ 26.71″	29°58′ 09.09″	2971	4.3	12.7	1209	213	1422	733	0	P/D/M
JR-3	101°56′ 47.35″	29°54′ 07.96″	3375	1.7	12.9	1239	219	1458	2167	0	B
JR-4	101°57′ 11.99″	29°54′ 36.40″	3301	2.2	3.0	1239	219	1458	274	8	B
JR-5	101°57′ 37.29″	29°56′ 06.67″	3138	3.2	11.4	1067	188	1256	2135	0	B/M/P
JR-6	101°55′ 33.09″	29°53′ 23.03″	3491	1.0	9.2	1239	219	1458	1936	0	B
Daduhe River basin											
DR-1	102°12′ 27.02″	29°38′ 46.24″	1265	15.0	46.5	330	58	388	1594	172	G
DR-2	102°12′ 28.33″	29°38′ 35.18″	1293	14.8	41.4	319	56	375	1997	46	G
DR-3	102°10′ 22.43″	29°29′ 51.47″	1022	16.5	10.1	281	50	330	589	0	G
DR-4	102°10′ 27.95″	29°33′ 30.85″	1108	16.0	3.5	287	51	338	158	0	G/S
DR-5	102°10′ 40.12″	29°33′ 40.40″	1153	15.7	8.7	316	56	371	290	90	G
DR-6	102°10′ 29.21″	29°34′ 49.31″	1157	15.6	13.4	312	55	367	506	90	G
DR-7	102°10′ 49.13″	29°35′ 50.89″	1165	15.6	1.5	335	59	394	69	3	G/D
DR-8	102°10′ 36.71″	29°36′ 19.98″	1167	15.6	1.0	278	49	327	4	0	G/D
Nanyahe River basin											
NR-1	102°10′ 12.46″	28°55′ 49.32″	2686	6.1	5.2	487	86	573	88	15	K/Q
NR-2	102°10′ 27.81″	28°55′ 45.61″	2689	6.0	2.0	357	63	419	25	0	K/Q
NR-3	102°13′ 10.41″	28°55′ 34.88″	2610	6.5	2.1	376	66	442	32	0	D/Q
NR-4	102°20′ 25.8″	29°05′ 04.47″	1380	14.3	6.3	330	58	389	208	29	D
NR-5	102°19′ 14.06″	29°02′ 34.74″	1602	12.9	6.3	329	58	387	76	19	G
NR-6	102°18′ 48.43″	29°01′ 52.75″	1650	12.6	2.7	349	62	410	235	70	G
NR-7	102°13′ 33.92″	28°55′ 33.77″	2539	7.0	14.7	380	67	448	40	0	D
NR-8	102°15′ 32.63″	28°57′ 13.36″	2242	8.9	3.2	406	72	478	52	19	D
NR-9	102°27′ 17.35″	29°06′ 03.94″	1783	11.7	1.5	368	65	433	109	15	G
NR-10	102°26′ 59.08″	29°06′ 46.24″	1642	12.6	0.6	355	63	418	121	28	G
NR-11	102°26′ 37.77″	29°07′ 33.60″	1523	13.4	1.4	351	62	413	120	22	G
NR-12	102°24′ 31.87″	29°09′ 55.78″	1209	15.3	5.4	344	61	405	502	9	G

[a] H = high flow season; L = low flow season.
[b] Instantaneous discharge measured when sampling.
[c] Lithology: G = granite; P = plagiogranite B = biotite granite; K = K-feldspar granite; D = diorite; M = metamorphic rock (slat, schist); Q = Quaternary (siliciclastic rock, gravel rock, clay); S = Shale.

2016). The influence of OH^- and H^+ on the charge balances of these nature waters is minor. The concentrations of total dissolved solids (TDS) of the streams are 19.3–461.0 mg/l, with an average of 111.0 mg/l. The EC trends to follow the pattern of TDS, ranging from 9 to 568 μs/cm. The SPM contents are highly variable from one sample to another, ranging from 0.1 to 6311 mg/l. The water temperatures measured at sample collection are 5.3–24.0 °C in high flow season and 0.1–10.0 °C in low flow season, respectively. Strong negative correlations are observed between the water temperatures and elevations in both high and low flow seasons. The pattern of cationic dominance based on mean values (in μmol/l) in the streams is in the following order: $Ca^{2+} > Mg^{2+} > Na^+ > K^+$. The results exhibit that Ca^{2+} alone accounts for 57.8%, and Ca^{2+} together with Mg^{2+} account for 79.3% of the total cations, which likely reflect the predominance of carbonate weathering. This is also supported by the mildly alkaline pH of these stream waters. Na^+ and K^+ account for 16.2% and 4.4% of the total cations, respectively. The dissolved SiO_2 concentrations vary from 59 to 606 μmol/l (averaging at 162 μmol/l), higher than the global average (127 μmol/l) (Meybeck, 2003), showing intense silicate weathering. The pattern of anionic dominance based on mean values (in μmol/l) is in the following order: $HCO_3^- > SO_4^{2-} > NO_3^- > Cl^- > F^-$. The dominant anion is HCO_3^-, which accounts for 82.5% of the total anions. SO_4^{2-}, NO_3^- and Cl^- account for 11.0%, 2.7% and 2.4% of the total anions,

Table 2
Chemical and isotopic compositions of the stream waters from the small catchments on the southeastern Tibetan Plateau, China.

Sample	Season[a]	pH	EC	T[b]	HCO_3^-	F^-	Cl^-	NO_3^-	SO_4^{2-}	SiO_2	K^+	Na^+	Ca^{2+}	Mg^{2+}	TZ^+	TZ^-	TDS[c]	SPM	$\delta^{18}O$-H_2O	δD-H_2O	NICB[d]
No.			μs/cm	°C	μmol/l												mg/l		vs. SMOW (‰)		%
Yajiahe River basin																					
WY-1	H	8.5	180	9.0	1328	4	25	23	358	124	62	112	905	85	2154	2095	168	1.5	−12.6	−87.9	1.4
WY-2	H	8.8	198	14.2	1301	7	52	14	319	174	106	312	772	121	2203	2012	168	85.4	−13.1	−91.3	8.7
	L	8.5	480	7.0	3068	48	351	23	292	606	147	1539	845	380	4136	4075	351	0.8	−13.1	−92.3	1.5
WY-3	H	8.8	178	14.7	1436	1	1	16	211	81	91	32	819	155	2071	1874	155	3.3	−11.7	−81.1	9.5
	L	7.4	256	1.2	1661	0	36	26	232	88	76	35	840	353	2498	2187	178	0.7	−13.1	−89.8	12.5
WY-4	H	8.8	230	16.8	1876	1	7	18	265	106	137	40	1048	195	2663	2433	201	9.9	−11.1	−74.9	8.6
	L	8.7	283	4.1	1856	0	36	31	178	113	99	39	915	412	2792	2279	192	1.0	−11.3	−77.3	18.4
WY-5	H	8.8	206	14.8	1878	1	7	18	177	77	71	26	1033	150	2464	2259	186	5.9	−12.0	−81.2	8.3
	L	8.3	283	4.2	2122	0	42	26	166	93	75	31	965	327	2690	2521	204	1.8	−11.8	−80.8	6.3
WY-6	H	8.9	264	17.4	2745	5	16	42	120	131	65	74	935	621	3251	3047	247	6311.0	−9.6	−66.5	6.3
	L	8.7	381	5.8	4025	16	49	34	133	140	44	107	808	1584	4935	4391	346	10.6	−10.1	−69.8	11.0
WY-7	H	8.8	267	17.7	1766	3	9	26	555	128	167	70	1028	426	3146	2914	230	1067	−10.1	−68.6	7.4
	L	8.7	568	4.0	4974	15	30	26	489	123	98	132	980	2243	6676	6024	461	1.2	−9.6	−69.0	9.8
WY-8	H	7.1	13	10.5	158	16	1	5	12	59	6	19	82	15	219	204	19	64.2	−12.3	−87.6	6.8
	L	7.3	94	4.6	742	62	28	27	39	280	10	94	277	126	909	936	86	0.2	−11.4	−76.6	−3.0
WY-9	H	8.2	114	10.8	921	20	24	23	99	167	26	156	502	54	1295	1185	104	0.3	−11.6	−79.3	8.5
	L	7.1	133	8.8	956	29	49	14	65	176	20	175	389	102	1178	1178	101	0.3	−10.7	−79.4	0.0
WY-10	H	8.7	196	10.1	2063	0	6	22	97	100	45	51	734	435	2434	2284	186	683.2	−10.9	−75.1	6.2
	L	7.6	283	2.0	2686	0	35	22	96	104	36	59	736	1029	3624	2935	239	0.3	−10.7	−75.3	19.0
WY-11	H	8.5	76	9.3	655	4	7	14	83	122	35	67	345	59	911	845	75	710.2	−14.1	−101.7	7.3
	L	7.3	170	2.2	1116	16	31	8	110	180	36	181	474	187	1538	1392	120	1.0	−12.7	−90.1	9.5
WY-12	H	8.5	125	11.0	1128	4	10	19	112	148	59	146	532	100	1469	1384	119	19.7	−11.7	−80.9	5.8
WY-13	H	8.6	193	13.5	513	0	5	8	693	85	69	56	832	120	2029	1911	144	3.1	−13.4	−95.0	5.8
	L	7.6	458	0.1	1871	0	34	22	965	105	69	81	1456	457	3977	3858	290	6.5	−14.7	−109.6	3.0
EY-1	H	7.9	13	9.0	200	1	1	10	11	92	4	32	70	22	220	233	24	0.5	−13.3	−95.5	−5.8
	L	7.6	20	0.7	167	8	26	24	33	119	5	39	63	56	283	291	28	0.2	−13.8	−100.3	−3.0
EY-2	H	7.6	13	9.3	156	1	3	8	11	95	7	32	68	17	209	191	21	1.3	−12.4	−86.5	8.6
	L	7.8	26	0.5	208	0	0	17	35	141	6	42	67	49	280	295	31	0.3	−12.2	−90.1	−5.5
EY-3	H	8.0	11	9.4	176	1	1	12	11	83	6	29	77	18	226	212	22	1.0	−12.1	−85.6	6.1
	L	7.6	27	0.4	222	0	25	18	34	133	8	45	76	55	315	332	32	0.2	−12.7	−90.5	−5.3
EY-4	H	7.9	13	8.0	186	1	1	12	13	80	6	26	79	19	228	227	23	8.4	−12.3	−86.0	0.4
EY-5	H	7.8	9	9.4	175	1	5	12	17	112	4	42	72	28	247	227	25	6.3	−12.4	−88.5	8.0
	L	8.3	25	0.3	246	12	26	23	34	195	4	49	68	78	344	376	38	0.3	−13.4	−94.3	−9.2
Jiazela River basin																					
JR-1	H	8.1	37	9.6	319	1	13	17	77	112	17	61	151	42	464	504	44	3.7	−15.2	−111.5	−8.6
	L	8.4	171	1.8	1870	15	194	18	72	187	42	704	456	444	2548	2240	188	0.3	−15.1	−109.4	12.1
JR-2	H	8.1	46	10.9	360	1	4	9	56	89	9	51	180	47	516	486	43	0.1	−14.9	−108.5	5.8
JR-3	H	8.2	38	7.3	314	6	6	16	54	80	12	39	192	24	482	450	40	1.2	−15.7	−114.5	6.7
JR-4	H	8.1	31	5.3	371	12	1	14	35	130	12	61	153	44	468	467	44	0.4	−14.7	−106.1	0.3
	L	7.3	77	0.3	576	21	27	21	52	177	11	80	192	167	807	749	67	0.2	−14.6	−107.3	7.3
JR-5	H	8.3	84	10.2	611	0	7	11	104	76	14	63	340	83	924	837	70	0.1	−14.6	−108.7	9.4
JR-6	H	7.5	143	9.6	1051	11	6	10	223	122	22	56	507	258	1610	1523	123	35.0	−16.5	−121.2	5.4
Daduhe River basin																					
DR-1	H	8.1	57	18.0	520	9	11	43	45	124	15	66	204	93	675	673	59	6.8	−10.3	−70.9	0.2
	L	7.4	94	8.7	742	21	35	55	48	140	11	95	225	243	1043	948	81	0.5	−11.0	−75.6	9.1
DR-2	H	7.9	47	16.1	413	6	9	50	43	146	19	78	151	80	558	563	52	179.7	−10.1	−67.7	−0.9
	L	7.6	117	10.0	966	32	36	53	70	207	21	144	247	302	1262	1227	105	0.3	−10.7	−73.0	2.7
DR-3	H	8.4	142	18.1	1031	75	14	86	130	205	20	156	510	198	1593	1465	124	10.8	−9.7	−66.4	8.0
DR-4	H	8.9	302	17.8	2371	38	31	177	283	426	114	676	550	680	3249	3183	269	372.6	−9.8	−69.7	2.0
DR-5	H	8.6	61	16.5	484	86	4	37	39	216	15	124	269	43	763	689	66	0.3	−10.1	−68.1	9.7
	L	7.6	81	8.8	530	56	29	50	47	185	10	113	192	165	837	759	68	0.3	−11.1	−75.3	9.3
DR-6	H	8.4	78	16.6	580	30	10	31	40	201	22	118	244	81	790	732	69	6.4	−9.9	−67.9	7.3
	L	7.4	70	8.8	452	93	27	36	42	215	7	113	183	79	644	692	62	1.7	−10.8	−69.5	−7.4
DR-7	H	8.5	97	22.5	702	16	15	30	102	245	48	163	287	127	1039	968	90	41.3	−10.3	−72.3	6.9
	L	7.2	172	7.8	1203	41	35	39	99	206	33	199	426	303	1690	1516	130	5.7	−11.5	−74.4	10.3
DR-8	H	8.4	234	24.0	1484	38	37	34	397	241	42	236	836	298	2547	2388	195	0.1	−9.6	−68.8	6.2
Nanyahe River basin																					
NR-1	H	8.4	29	11.6	280	2	7	24	27	124	5	55	120	43	386	367	36	0.3	−12.0	−86.8	4.9
	L	7.3	38	3.8	314	14	31	48	41	130	3	51	100	97	449	490	43	2.5	−12.5	−88.7	−9.2
NR-2	H	7.8	16	10.0	120	1	8	42	25	112	5	42	65	22	221	222	24	0.2	−10.8	−78.1	−0.2
NR-3	H	7.8	22	14.4	200	0	7	12	33	129	11	44	69	53	299	284	30	1.3	−11.1	−76.7	5.1
NR-4	H	7.8	57	16.4	440	13	18	58	66	215	24	114	227	55	702	662	65	4.0	−10.2	−69.3	5.7
	L	8.0	151	8.4	1143	32	54	133	59	270	34	203	362	313	1585	1479	130	5.2	−9.4	−67.0	6.7
NR-5	H	7.7	82	17.7	650	46	12	25	99	195	28	118	362	63	996	931	84	3.7	−10.1	−68.7	6.5
	L	7.2	118	6.4	725	81	37	40	80	200	21	143	324	157	1126	1042	90	0.5	−9.7	−68.8	7.5
NR-6	H	7.8	79	14.6	607	6	10	26	88	179	20	88	364	46	928	825	77	3.3	−10.4	−70.0	11.1
	L	7.3	113	6.4	773	23	34	46	87	182	14	90	349	112	1027	1050	90	0.8	−10.4	−71.0	−2.3
NR-7	H	8.5	94	10.0	513	0	10	15	180	161	18	66	316	124	963	898	77	0.6	−11.2	−75.9	6.8
NR-8	H	8.6	112	13.1	927	1	11	18	111	151	49	82	454	106	1252	1179	102	2.0	−11.2	−77.6	5.8
	L	7.3	135	2.8	999	0	40	34	81	132	36	77	389	234	1358	1235	105	178.7	−11.2	−78.9	9.1

(*continued on next page*)

Table 2 (*continued*)

Sample	Season[a]	pH	EC	T[b]	HCO_3^-	F^-	Cl^-	NO_3^-	SO_4^{2-}	SiO_2	K^+	Na^+	Ca^{2+}	Mg^{2+}	TZ^+	TZ^-	TDS[c]	SPM	$\delta^{18}O$-H_2O	δD-H_2O	NICB[d]
No.			μs/cm	°C	μmol/l												mg/l		vs. SMOW (‰)		%
NR-9	H	7.3	58	17.5	149	12	25	89	153	190	22	100	173	86	639	581	54	1.4	−10.9	−75.8	9.1
	L	7.2	71	7.5	314	35	60	81	68	256	17	138	114	128	640	626	60	0.3	−9.8	−67.8	2.1
NR-10	H	7.6	64	14.4	443	5	42	30	110	197	21	137	190	113	762	740	67	3.1	−10.5	−74.5	3.0
	L	8.0	48	7.7	333	17	35	85	44	231	8	116	85	123	538	557	55	2.2	−10.2	−73.1	−3.4
NR-11	H	7.7	85	17.1	684	19	37	26	140	202	27	158	301	134	1055	1045	91	2.2	−10.5	−74.0	1.0
	L	6.9	131	6.9	873	26	76	91	75	224	25	202	254	323	1382	1216	106	0.3	−10.2	−72.3	12.0
NR-12	H	8.4	86	20.0	855	27	9	10	83	183	25	95	459	44	1126	1067	95	17.6	−10.3	−73.7	5.3
	L	6.9	150	8.8	1142	41	56	46	54	206	14	202	449	144	1400	1393	120	0.8	−10.3	−70.7	0.5

[a] H = high flow season; L = low flow season.
[b] Water temperature.
[c] TDS = total dissolved solid = $Na^+ + K^+ + Mg^{2+} + Ca^{2+} + Cl^- + SO_4^{2-} + NO_3^- + HCO_3^- + SiO_2$.
[d] NICB = normalized inorganic charge balance = $(TZ^+ - TZ^-)/TZ^+ \times 100\%$.

respectively. The ionic compositions are comparable to the other granitic catchments (White and Blum, 1995; Millot et al., 2002; Oliva et al., 2003; West et al., 2005 and Fernandes et al., 2016). Low concentrations of F^-, NO_3^- and Cl^- for most samples suggest that the anthropogenic influence on the water geochemistry is limited in the small catchments. Poor relationship between $[Cl^-]$ and $[SO_4^{2-}]$ is observed ($R^2 = 0.01$), indicating the evaporites dissolution is negligible as evaporite contributions would likely co-exist with high-sulfate salts, leading to a good correlation between $[Cl^-]$ and $[SO_4^{2-}]$ (Turchyn et al., 2013).

4.1.1. Seasonal variations

Seasonal variations of hydro-geochemistry are mainly caused by various climatic conditions and the resulting hydrological and chemical processes. The pH values are found to be slightly lower in low flow season than in high flow season. In general, the SPM contents are higher in high flow season than in low flow season. The considerable variability of TDS is shown by the high standard deviations i.e., 96 ± 67 mg/l and 133 ± 103 mg/l during the high and low flow seasons, respectively. The coupled effects of high precipitation and intense melting of glaciers result in high discharge, which is supposed to be responsible for the lower concentrations of dissolved components in high flow season (Hindshaw et al., 2011).

The discharge ranges from 4 to 2860 l/s in high flow season and 0 to 480 l/s in low flow season, respectively. The discharge varies by an average factor of 60 (up to 770) over the high and low flow seasons, whereas the maximum TDS variation is only a factor of 4 (WY-8), which demonstrates that the variability in solute concentrations is not only controlled by dilution. The dilution effect from increasing runoff is supposed to be counterbalanced by increasing chemical weathering fluxes. The Ca/Si ratios of the small catchments vary by factors of 0.3–13.8 in different seasons, with higher values observed in high flow season. The seasonal change of Ca/Si ratios has also been observed in other catchments (Hosein et al., 2004; Tipper et al., 2006; Gabet et al., 2010), which is likely to be caused by the changing proportion of carbonate to silicate weathering as proposed by Tipper et al. (2006) for Himalayan rivers.

The $\delta^{18}O$ and δD of the stream water samples vary from −16.5‰ to −9.6‰ (averaging at −11.7‰) and −121.2‰ to −66.4‰ (averaging at −82.4‰) in high flow season, and from −15.1‰ to −9.4‰ (averaging at −11.7‰) and −109.6‰ to −66.4‰ (averaging at −82.1‰) in low flow season, respectively (Table 2).

4.1.2. Spatial variations

Although the studied catchments are located in a small area, the obvious spatial differences of hydro-geochemistry are observed. The SPM contents of the streams draining WY are relatively high as they drain large areas of fine grained material deposited from the glacier moraines. In general, streams draining granitoids lithologies (e.g., EY and NR) have lower TDS and EC than those draining mixed lithologies. Some samples (e.g., WY-2 and JR-1) display relatively higher concentrations of Na^+ and Cl^-, especially in low flow season, which are probably due to the contribution of hot springs nearby.

The Ca/Na and Ca/Si molar ratios show distinct value ranges between streams draining pure granitoids (e.g., EY) and mixed lithologies (e.g., WY), with higher ratios for the streams draining mixed lithologies. In addition, differences in Ca/Si and Ca/Na ratios are also observed for the streams draining granitoids lithologies. The complex and varied spatial responses of the ratios are due to different solute sources (e.g., preferential carbonate weathering) (Hindshaw et al., 2011). Blum et al. (1998) showed that trace carbonates are present in silicate rocks and contribute strongly to the chemical signature of rivers despite of their low abundance.

The equation of the local stream water line in the region is:

$$\delta D = 7.82\,\delta^{18}O + 9.42\ (R^2 = 0.97) \quad (1)$$

The streams at high elevations are depleted in ^{18}O compared with those at low elevations (Tables 1 and 2). The highest $\delta^{18}O$ value is observed for the JR-6 in high flow season and the lowest is observed for the NR-4 in low flow season. The differences may due to different water sources (e.g., glacier meltwater and rain water) and evaporation processes (Clark and Fritz, 1997).

4.2. Water geochemistry of precipitation, glacier meltwater and spring water

The chemical and isotopic compositions of the precipitation, glacier meltwaters and spring waters are presented in Table 3. The chemical compositions of the precipitation are different and significant seasonal variations can be observed. The ion concentrations for the precipitation are relatively low in high flow season. In generally, Ca^{2+} is the most abundant ion among the major cations. SO_4^{2-} and NO_3^- are dominant among the major anions. The volume-weighted mean concentration of Cl^- for the precipitation is 0.55 μmol/l in high flow season and 12.7 μmol/l in low flow season. The element to chloride ratios also show significant seasonal variations (shown in Table 3). The volume-weighted average $\delta^{18}O$ and δD for the precipitation in high flow season (−9.6‰ and −58.5‰) are depleted in ^{18}O and D compared with those in low flow season (−7.2‰ and −48.5‰). The $\delta^{18}O$ ratio of the precipitation is enriched in ^{18}O compared with the stream waters. (Tables 2, 3 and Fig. 2). The $\delta^{18}O$ are plotted against δD for local precipitation samples to obtain the Local Meteoric Water Line (LMWL):

$$\delta^{18}O = 7.68\,\delta D + 10.72\ (R^2 = 0.97) \quad (2)$$

The stream water line has similar slop with the LMWL (Fig. 2), indicating the absence of significant evaporation and oxygen isotope exchanges (Clark and Fritz, 1997; Schulte et al., 2011; Hagedorn and Whittier, 2015), which might be an implication of the humid climate

Table 3
Chemical and isotopic compositions of the glacier meltwaters, springs, precipitations and ground waters collected in the study area.

Catchment No.	Longitude (E)	Latitude (N)	Cl^-	NO_3^-	SO_4^{2-}	K^+	Na^+	Ca^{2+}	Mg^{2+}	$\delta^{18}O$-H_2O	δD-H_2O	$[K^+]/[Cl^-]$	$[Na^+]/[Cl^-]$	$[Ca^{2+}]/[Cl^-]$	$[Mg^{2+}]/[Cl^-]$
			μmol/l							vs. SMOW (‰)					
Glacier															
Gla-1	101°58′42.36″	29°33′50.04″	5.2	7.9	11.5	2.4	5.8	14.2	1.5	−17.1	−124.4	0.46	1.10	2.70	0.29
Gla-2	101°58′31.97″	29°33′37.79″	8.8	7.4	11.2	3.7	18.5	8.1	1.9	−16.4	−117.3	0.42	2.09	0.92	0.21
Gla-3	101°58′17.78″	29°33′30.80″	4.9	7.3	0.0	3.5	4.6	18.8	1.6	−16.0	−110.1	0.72	0.94	3.86	0.34
Average			6.3	7.5	7.6	3.2	9.6	13.7	1.7	−16.5	−117.3	0.53	1.38	2.49	0.28
Spring															
High flow season															
S-1	102°01′46.27″	29°35′21.00″	1115.9	114.0	585.2	488.5	6091.8	1379.4	217.1	−14.1	−102.6	0.44	5.46	1.24	0.19
S-2	102°00′24.11″	29°42′14.81″	1267.2	110.8	30.8	368.4	5924.7	1022.4	192.6	−12.5	−88.5	0.29	4.68	0.81	0.15
S-3	102°03′35.88″	29°45′16.12″	2364.0	146.3	140.9	221.5	11,083.0	740.8	590.7	−14.2	−102.9	0.09	4.69	0.31	0.25
S-4	101°57′09.63″	29°58′46.06″	7070.5	702.3	-	1440.0	23,466.7	93.9	1158.1	−15.4	−123.5	0.20	3.32	0.01	0.16
S-5	101°57′17.02″	29°58′32.97″	7726.4	184.5	48.1	1315.9	21,177.4	143.9	293.2	−14.8	−120.1	0.17	2.74	0.02	0.04
S-6	102°08′15.62″	29°32′08.88″	6182.1	132.0	1429.0	993.1	13,908.5	3166.5	1242.5	−10.7	−78.4	0.16	2.25	0.51	0.20
Low flow season															
S-1	102°01′46.27″	29°35′21.00″	1889.2	-	590.2	300.3	8052.9	445.1	460.6	−15.6	−118.5	0.16	4.26	0.24	0.24
S-2	102°00′24.11″	29°42′14.81″	2118.7	99.2	343.9	165.3	4914.9	254.4	330.6	−13.0	−89.3	0.08	2.32	0.12	0.16
S-3	102°03′35.88″	29°45′16.12″	2373.3	136.5	392.6	100.2	10,245.7	157.1	1050.0	−15.5	−107.7	0.04	4.32	0.07	0.44
S-4	101°57′09.63″	29°58′46.06″	6550.2	321.5	-	595.4	21,814.7	83.0	2611.4	−15.5	−123.3	0.09	3.33	0.01	0.40
S-5	101°57′17.02″	29°58′32.97″	6401.5	95.9	298.0	602.0	22,155.0	134.7	1693.5	−16.2	−125.1	0.09	3.46	0.02	0.26
S-6	102°08′15.62″	29°32′08.88″	6215.2	-	926.1	460.4	14,064.3	643.4	3055.1	−10.7	−80.2	0.07	2.26	0.10	0.49
Precipitation															
High flow season															
P-1 (43 mm)	101°59′54.00″	29°34′34.00″	-	9.3	15.1	1.2	4.7	18.4	4.0	−7.8	−49.5	-	-	-	-
P-2 (28 mm)			-	10.8	10.0	1.2	20.1	11.4	0.8	−7.7	−48.6	-	-	-	-
P-3 (22 mm)			3.7	9.1	10.9	1.3	6.0	12.7	3.1	−7.3	−49.7	0.35	1.62	3.45	0.85
P-4 (57 mm)			-	9.2	12.0	1.1	4.7	10.3	1.7	−12.7	−87.8	-	-	-	-
Volume-weighted average			0.5	9.6	12.5	0.9	6.1	9.9	2.1	−9.6	−58.5	1.60	11.14	18.13	3.75
Low flow season															
P-1 (4.2 mm)	101°59′54.00″	29°34′34.00″	14.1	44.4	24.5	2.2	1.5	10.6	1.7	−9.1	−59.6	0.16	0.11	0.75	0.12
P-2 (4.6 mm)			14.2	47.2	20.2	1.7	2.2	15.3	4.7	−5.1	−47.1	0.12	0.15	1.08	0.33
P-3 (0.4 mm)			14.3	29.7	17.8	1.8	1.7	5.2	1.3	−9.3	−61.4	0.12	0.12	0.36	0.09
P-4 (1.4 mm)			2.5	39.0	37.0	1.7	1.7	17.6	3.7	−6.9	−39.8	0.70	0.67	7.06	1.50
P-5 (2.4 mm)			7.7	44.2	43.7	3.2	5.0	18.4	3.7	−6.7	−40.2	0.42	0.64	2.37	0.48
P-6 (3.0 mm)			14.6	41.2	25.4	1.1	1.6	12.8	2.4	−8.9	−52.4	0.07	0.11	0.87	0.17
P-7 (4.2 mm)			14.4	36.9	58.8	2.6	1.7	9.0	2.4	−6.7	−42.5	0.18	0.12	0.62	0.17
Volume-weighted average			12.7	42.3	33.8	2.1	2.1	13.0	3.0	−7.2	−48.5	0.16	0.17	1.02	0.24
Ground water															
GW-1	102°10′12.93″	29°36′17.24″								−10.0	−75.6				
GW-2	102°09′39.86″	29°36′20.84″								−10.0	−75.4				
GW-3	102°01′54.42″	29°42′13.91″								−9.2	−72.3				
Average										−9.7	−74.4				

-: not detected/calculated.

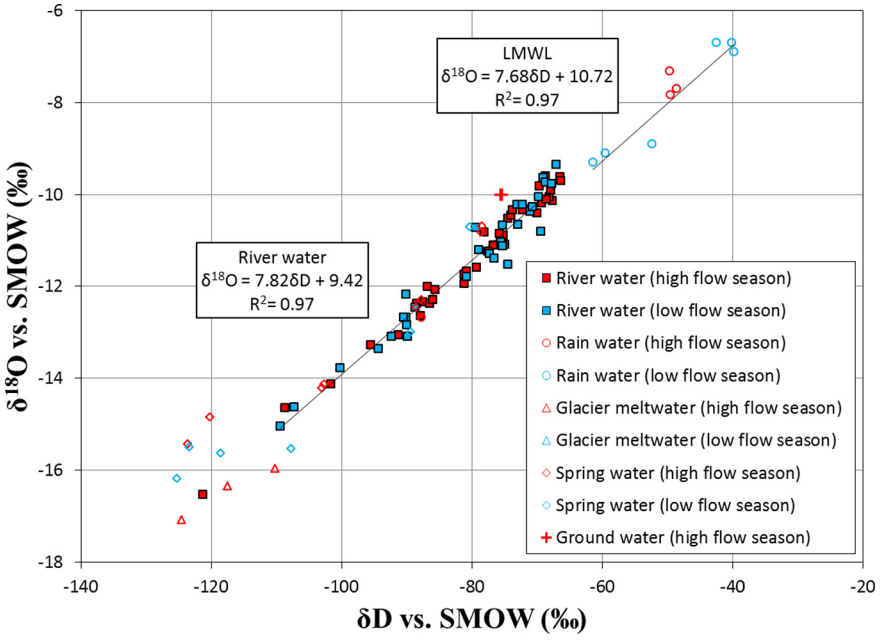

Fig. 2. The $\delta^{18}O$ and δD values of the stream waters, local precipitation, hot spring waters and glacier meltwaterwaters. The Local Meteoric Water Line (LMWL) has almost the same slop with the stream water line, indicating a lack of significant evaporation and oxygen isotope exchanges.

and short residence time of waters.

The glacier meltwater samples are dilute. The dominant cation is Ca^{2+}. Cl^-, NO_3^- and SO_4^{2-} are the main anions. The average Cl^- concentration for the glacial meltwater is 6.3 ± 1.8 μmol/l, showing a narrow range. The chemical composition of glacier meltwater varies due to preferential leaching and fractionation of ions (Johannessen and Henriksen, 1978; Williams and Melack, 1991; Marsh and Pomeroy, 1999) and this will result in non-constant element to Cl^- ratios. However, the preferential elution of Cl^- is much less pronounced (Williams and Melack, 1991; Marsh and Pomeroy, 1999), resulting in little variation of Cl^- concentrations of the glacial meltwaters. Variations of the elements to chloride ratios are presented in Table 3. The $\delta^{18}O$ and δD of the glacial meltwaters vary from −17.1‰ to −16.0‰ (averaging at −16.5‰) and −124.4‰ to −110.1‰ (averaging at −117.3‰), respectively, also showing a narrow range. The isotopic $\delta^{18}O$ ratios of the glacial meltwaters are depleted in ^{18}O compared with the stream waters (Fig. 2).

The hot spring waters are characterized by high TDS and major ions concentrations. The elements of the hot springs may have a magmatic origin, may from rock leaching, or may illustrate the influence of respiring bacteria (Dessert et al., 2009). The Na^+ displays the highest concentrations among the cations in the spring waters. After HCO_3^-, Cl^- is the most abundant anion. The average Na^+ and Cl^- concentrations are similar in different seasons, with 13,609 and 4288 μmol/l in high flow season and 13,541 and 4258 μmol/l in low flow season, respectively. The K^+, SO_4^{2-}, Ca^{2+} and Mg^{2+} concentrations are relatively low in the spring waters. The $\delta^{18}O$ and δD of the spring waters show a wide range. The isotopic $\delta^{18}O$ ratios range from −10.7‰ to −15.4‰ and −10.7‰ to −16.2‰ in high and low flow seasons, respectively. The spring waters in low flow season are depleted in ^{18}O compared with those in high flow season. Spatially, the hot springs show significant differences in their chemical signatures. The two springs (S-1 and S-2) collected in WY have low ionic concentrations. However, the $[Cl^-]$-normalized ratios are generally high due to the low Cl^- concentrations. The springs S-1 and S-2 present similar ionic concentrations, lower than those of the springs collected in JR (S-4 and S-5). The two springs in JR are highly enriched in Na^+ (21,000–23,000 μmol/l), K^+ (1300–1400 μmol/l) and Cl^- (6400–7700 μmol/l) and depleted in Ca^{2+} (80–140 μmol/l). The spring S-6 collected in DR has higher SO_4^{2-}, Ca^{2+} and Mg^{2+} concentrations than other springs. The springs collected at high elevations are depleted in ^{18}O compared with those collected at lower elevations. Since the stream waters are dilute, the dissolved loads could be significantly influenced by the hot spring waters.

4.3. Major element composition of bed rock samples

The major element compositions of the bedrock samples from the small catchments are presented in Table 4. The loss on ignition (LOI) is generally < 2%. The granitoids have K_2O, Na_2O, CaO, MgO and SiO_2 contents of 1.4–5.6, 2.2–4.9, 1.1–4.9, 0.1–2.3 and 62.3–75.6 wt%, respectively. All the granitoids analyzed from the catchments are enriched in Al_2O_3 (12.2–16.1 wt%). Low Na_2O/K_2O ratios (averaging at 0.66), MgO (averaging at 0.8 wt%) and CaO contents (averaging at 1.8 wt%) are observed for the granitoids collected in NR. They are generally peraluminous, with aluminium saturation indexes (ASI) (Shand, 1927) of 1.0–1.1 (Table 4). The granitoids collected in other catchments (e.g., WY and JR) are generally metaluminous (ASI < 1), with high Na_2O/K_2O ratios (averaging at 1.8), MgO and CaO contents (averaging at 1.3 and 3.1 wt%, respectively). The results are in accordance with the fact that the granitoids in NR contain enclaves composed of biotite and quartz, and contain less dark minerals than those collected in other catchments (Table 4). The Ca/Na and Mg/Na molar ratios of the granitoids range from 0.14 to 0.78 (averaging at 0.42) and 0.02 to 0.62 (averaging at 0.25), respectively. The schists (plagioclase-amphibole schist) collected in WY are rich in amphibole. The plagioclase-amphibole schists have average K_2O, Na_2O, CaO, MgO and SiO_2 contents of 1.2, 2.7, 8.0, 4.7 and 55.4 wt%, respectively. The average Ca/Na and Mg/Na molar ratios are 1.62 and 1.34, respectively. Based on the hand specimen observation and the chemistry data, it is assumed that the mobile elements of the rock samples have not been leached out by weathering reactions.

5. Discussions

Hydro-geochemical investigations can provide insightful information on water mixing processes and solute sources. However, end-members identification is the premise. Based on mass balance and

Table 4
Chemical compositions of the silicate bedrocks collected in the study area.

Sample No.	Al_2O_3	CaO	TFe_2O_3	K_2O	MgO	MnO	Na_2O	P_2O_5	SiO_2	TiO_2	LOI	Ca/Na	Mg/Na	ASI[a]	Descriptions[b]
	wt%											Molar ratio			
Metamorphic rocks															
M-1	12.0	7.4	10.5	1.3	4.7	0.2	2.7	0.2	58.3	1.9	0.3	1.49	1.32	0.62	Plagioclase-amphibole schist: amphibole > 40%
M-2	17.3	8.5	9.9	1.0	4.8	0.2	2.7	0.2	52.5	0.9	1.4	1.75	1.36	0.82	
Average												1.62	1.34		
Granitoids															
G-1	16.1	4.5	4.5	1.9	1.9	0.1	4.1	0.1	64.6	0.4	1.6	0.62	0.35	0.95	Plagiogranites:andesine and plagioclase 55–75%, quartz
G-2	15.0	3.7	4.7	2.0	1.6	0.1	3.9	0.1	67.0	0.5	1.4	0.53	0.33	0.98	20–30%, microcline 0–15%, biotite ca. 5%.
G-3	18.1	4.9	4.8	1.4	1.6	0.1	4.9	0.2	62.7	0.6	0.2	0.55	0.25	0.97	
G-4	13.5	3.2	2.7	3.5	1.1	0.1	3.2	0.2	70.9	0.4	1.2	0.56	0.28	0.91	
G-5	12.9	1.7	1.3	3.5	0.4	0.0	3.5	0.1	75.6	0.2	0.5	0.27	0.08	1.01	
G-6	12.2	2.6	2.7	2.0	1.2	0.1	4.0	0.1	72.2	0.3	2.5	0.36	0.24	0.90	Biotite granite: microcline and oligoclase 60%, quartz
G-7	12.8	3.5	4.3	2.3	1.7	0.1	2.5	0.1	68.6	0.6	3.3	0.78	0.52	0.99	20–30%, biotite 8–15%.
G-8	15.1	3.3	9.2	1.9	1.1	0.3	4.6	0.3	62.3	0.9	0.8	0.40	0.18	0.96	Granites: K-feldspar 30–60%, plagioclase 15–40%, quartz
G-9	14.3	1.2	3.4	2.5	1.0	0.0	4.7	0.1	70.7	0.4	1.5	0.14	0.16	1.12	20–40%, biotite 1–3%.
G-10	15.3	2.6	3.8	2.6	1.2	0.1	4.9	0.1	67.5	0.5	0.8	0.29	0.18	0.98	
G-11	14.2	3.0	4.3	3.5	1.9	0.1	2.2	0.1	64.7	0.5	5.2	0.74	0.65	1.10	
G-12	13.1	1.4	2.5	4.7	0.4	0.1	2.9	0.1	73.9	0.3	0.8	0.27	0.09	1.05	Granites: microperthite 45–50%, quartz 25–30%, oligoclase
G-13	13.5	1.6	3.0	4.8	0.4	0.1	3.0	0.1	72.3	0.3	1.0	0.30	0.11	1.03	15–20% and biotite ca. 3%, with enclaves composed of
G-14	14.8	1.8	3.6	4.9	0.5	0.1	3.4	0.1	69.6	0.4	1.3	0.28	0.11	1.05	biotite and quartz. Low Na_2O/K_2O ratios, low MgO, CaO
G-15	13.7	1.1	3.1	5.0	0.5	0.1	3.2	0.1	72.1	0.4	1.1	0.20	0.11	1.08	contents. Generally peraluminous.
G-16	15.7	3.9	5.5	3.6	2.3	0.1	2.9	0.2	63.7	0.7	1.6	0.74	0.61	0.99	
G-17	12.6	1.2	2.2	4.9	0.3	0.1	3.0	0.1	74.9	0.2	0.8	0.23	0.07	1.00	
G-18	15.1	1.3	0.8	5.6	0.1	0.0	3.1	0.0	72.2	0.1	1.8	0.23	0.03	1.12	
G-19	15.7	2.2	4.8	4.3	1.9	0.1	3.2	0.2	65.9	0.7	1.5	0.39	0.46	1.13	
Average												0.42	0.25		

[a] ASI = $Al_2O_3/(CaO + Na_2O + K_2O)$ (in mol, Shand, 1927).
[b] Geological Bureau of Sichuan Province (1974a, 1974b, 1977).

modeling approaches, efforts are made to constrain the end-members characterization, to quantify the contribution of the different sources to the stream runoff and solutes, and to estimate the weathering rates of these small catchments on the southeastern Tibetan Plateau.

5.1. Hydrograph separation

The understanding of hydrological process in a catchment is an important step to gain a better understanding of solutes sources (Hagedorn and Whittier, 2015). Water mixing processes of different reservoirs recharging stream runoff can be assessed with various tracers including major ions (e.g., Cl^-), stable isotopes (e.g., $\delta^{18}O$, δD) and radioactive isotopes (e.g., ^{14}C, ^{222}Rn) (Malard et al., 1999; Ladouche et al., 2001; Uhlenbrook and Hoeg, 2003; Liu et al., 2004; Liu et al., 2008; McCallum et al., 2010; Cartwright et al., 2011). The stream waters in alpine or mountainous area can be recharged by various water sources, such as precipitation, glacier meltwater, spring water, groundwater and frozen soil meltwater (Uhlenbrook and Hoeg, 2003; Zhang et al., 2012; Li et al., 2014b). Liu et al. (2010) proposed that water recharge from the groundwater is insignificant in the hydrological study of Hailuogou, a sub-basin of WY (Fig. 1). Besides, precipitation recharges the stream runoff mainly in terms of surface water or ground water (Li et al., 2014b). The $\delta^{18}O$ values of the ground waters collected in July (−9.2‰ to −10‰, averaging at −9.7‰) are similar to the values of the precipitation (volume-weighted averaging at −9.6‰), which implicates that ground water is the result of fast recharging of precipitation. Therefore, an assumption is proposed that the recharging discharge from groundwater to the stream could be amalgamated into precipitation input in the hydrograph separation approach for the studied catchments. Liu et al. (2010) and Zhang et al. (2012) proposed that glacier meltwater was a significant source of stream water of the Hailuogou. In addition, the high Cl^- concentrations of many stream waters (higher than the precipitation and glacier meltwaters) (Tables 2 and 3) indicate the inputs from Cl^--rich hot springs in the area. Since there are no evaporites according to geological surveys, and anthropogenic inputs are negligible in this pristine area, the stream water and the riverine Cl^- are mainly from glacier meltwater, precipitation and spring water. By combining $\delta^{18}O$ and Cl^- concentrations, contributions of major sources to stream discharge and Cl^- can be calculated as follows (Turner et al., 1992; Zhou et al., 2015):

$$[Cl^-]_{str} = a \times [Cl^-]_{pre} + b \times [Cl^-]_{gla} + c \times [Cl^-]_{spr} \quad (3)$$

$$\delta^{18}O_{str} = a \times \delta^{18}O_{pre} + b \times \delta^{18}O_{gla} + c \times \delta^{18}O_{spr} \quad (4)$$

$$a + b + c = 1 \quad (5)$$

The subscript str, pre, gla and spr represent stream, precipitation, glacier and spring, respectively. The contributions of each source to the stream discharge are denoted by a, b, c. The dissolved loads of small stream could be significantly influenced by a single precipitation event since the residence time of water is rather short. It is more appropriate to use the chemical and isotopic compositions of the precipitation collected during the sampling period. The volume-weighted mean Cl^- concentration and $\delta^{18}O$ of the precipitation are applied in the calculations, assuming that the chemical compositions of precipitation are homogeneous throughout the small studied area. The average Cl^- concentration and $\delta^{18}O$ of the glacial meltwaters are applied in the calculations since they show a narrow range. The hot spring waters show significant differences in the chemical compositions and seasonal variations (Table 3). Precise estimation of the hot spring contribution is rather difficult. In this study, for the catchments in which hot spring was collected, the chemical and isotopic compositions of the hot spring are applied (e.g., S-1 for WY-2 and S-4 for J-1). For the catchments in which no spring sample was collected, the nearest spring is applied (e.g., S-3 for the catchments of EY and S-6 for the catchments of DR and NR). Then the contributions of each runoff components are calculated according to the mass balance equations (Eqs. (3)–(5)). Some samples (WY-3, WY-8, EY-1, EY-3, EY-4, and JR-4 in high flow season) have extremely low Cl^- concentrations (~1 μmol/l) and $\delta^{18}O$ values between those of the glacier and precipitation, indicating glacier

meltwater and precipitation as the water sources. WY-6 in high flow season has similar $\delta^{18}O$ to that of precipitation and high Cl^- concentration, suggesting spring and precipitation to be the water sources. The water sources of these catchments are calculated using two end-member mixing model:

$$[Cl^-]_{str} = a \times [Cl^-]_{pre} + b \times [Cl^-]_{gla\ (spr)} \quad (6)$$

$$a + b = 1 \quad (7)$$

In addition, JR-6 in high flow season has similar Cl^- concentration and $\delta^{18}O$ value with glacier meltwater, indicating that the stream water is mainly recharged by glacier. EY-2 in low flow season has lower Cl^- concentration than all the end-members, and the stream water is assumed to be from precipitation.

The calculated results are given in Appendix A and Fig. 3. Stream waters are mainly recharged by precipitation and glacier meltwater. Glacier meltwater contributes 0.1–100% (averaging at 25.8%) and 0–81.9% (averaging at 44.4%) of the total discharge in high and low flow season, respectively. The highest glacier meltwater contributions are found for the small catchments of JR, a typical glacial basin. For the sub-mountain catchments (e.g., small catchments of DR and NR), the contributions of glacier meltwater are small in high flow season but increases significantly in low flow season. Precipitation accounts for 0–99.3% (averaging at 73.9%) of the total discharge in high flow season and 15.3–100% (averaging at 54.1%) in low flow season, respectively. High precipitation contributions are observed for the small catchments of DR and NR. Spring contributes 0.8% of the total discharge on average. The highest contributions (4.3% in high flow season and 18.2% in low flow season) are observed for WY-2.

Based on the LSM-simulated runoff and the hydrograph separation results, precipitation contributes 323–342 mm, while glacial meltwater contributes 4–1450 mm to the annual runoff of the small catchments. The simulated annual runoff results are compared to the GAEOS gauge-observed runoff data in Fig. 4. The average annual runoff of WY-1 and WY-13 were 605 (556–657) mm and 420 (227–659) mm during 2003–2007, respectively (the GAEOS monitoring data). The LSM simulated eight-year series annual average runoff are 587 mm for WY-1 and 436 mm for WY-13, respectively. The simulation and observing results matched well, with errors at 3% for WY-1 and 4% for WY-13, respectively. Propagated uncertainties are considered when using these results in the calculation of chemical weathering rates in the following sections.

5.2. Sources of solutes

The dissolved species of the stream water are the products of mineral weathering, precipitation, glacier and spring inputs in the drainage basin. A forward method is employed in this study to quantify the contribution of each reservoir (Galy and France-Lanord, 1999; Moon et al., 2007; Xu and Liu, 2010). The concentration of any element X in the dissolved load (in mol) can be written as the following equation:

$$[X]_{str} = [X]_{pre} + [X]_{gla} + [X]_{spr} + [X]_{sil} + [X]_{carb} \quad (8)$$

The subscript str, pre, gla, spr, sil and carb represent stream, precipitation, glacier, spring, silicate and carbonate, respectively. It is important to constrain the contributions of these sources to the dissolved loads to derive chemical weathering rates of the catchments.

5.2.1. Precipitation, glacier and spring inputs

Chloride (Cl^-) is the most common used reference to evaluate solute inputs to rivers (Négrel et al., 1993; Gaillardet et al., 1997). The portions of [Cl^-] from precipitation, glacier and spring water can be calculated by the end-member mixing model as discussed above (Eqs. (3)–(7)). Based on the contribution of [Cl^-] and the [Cl^-]-normalized elemental ratios of end-members for precipitation, glacier and spring water (Table 3), the corresponding contributions of other elements (X = Na^+, K^+, Ca^{2+} and Mg^{2+}) (in mol) can be calculated:

$$[X]_i = ([X]/[Cl^-])_i \times [Cl^-]_i \quad (9)$$

The subscript i stands for precipitation, glacier and spring water.

5.2.2. Chemical weathering inputs

After correction of the precipitation, glacier meltwater and spring water inputs, all the remaining [Na^+] and [K^+] are assumed to be from silicate weathering. [Ca^{2+}] and [Mg^{2+}] deriving from silicate weathering ($[Ca^{2+}]_{sil}$ and $[Mg^{2+}]_{sil}$) can be calculated as follows:

$$[Ca^{2+}]_{sil} = [Na^+]_{sil} \times (Ca/Na)_{sil} \quad (10)$$

$$[Mg^{2+}]_{sil} = [Na^+]_{sil} \times (Mg/Na)_{sil} \quad (11)$$

where $(Ca/Na)_{sil}$ and $(Mg/Na)_{sil}$ are the molar ratios of silicate end-member. Previous studies reported the $(Ca/Na)_{sil}$ and $(Mg/Na)_{sil}$ ratios in different ranges. White and Blum (1995) compiled small catchments draining granitoids and the $[Ca^{2+}]/[Na^+]$ ratios ranged between 0.03 and 3. In the world's large rivers, $(Ca/Na)_{sil} = 0.35 \pm 0.15$ and (Mg/

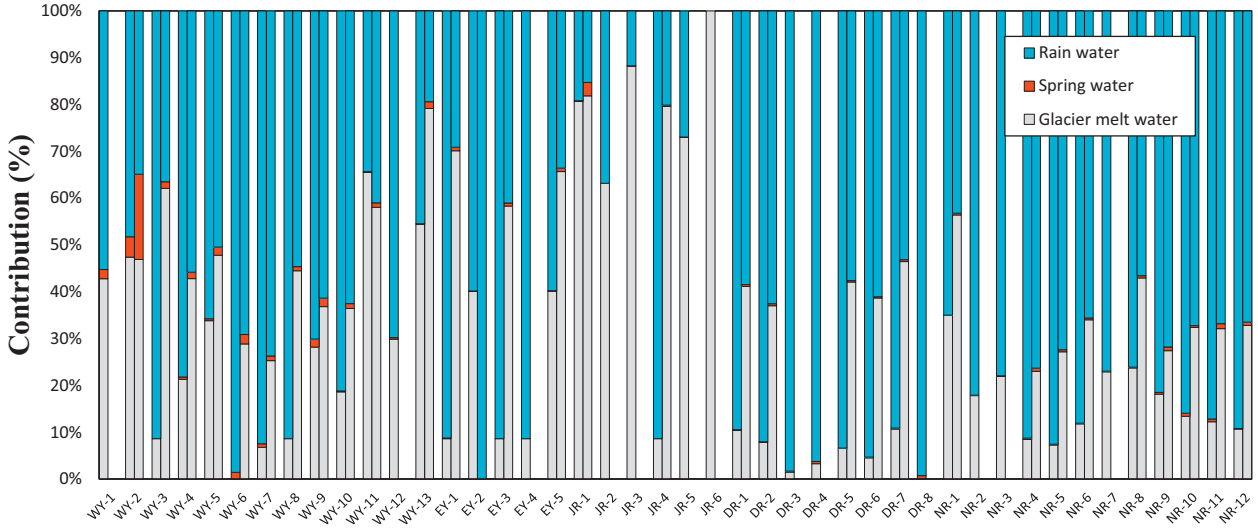

Fig. 3. Diagram showing the proportional contributions of each reservoir to the stream discharge in high flow season (left bar for a specific sample) and low flow season (right bar for a specific sample). All the streams were collected for high flow season samples, but some of them lack low flow season samples due to the absence of flow. The samples with only one bar are for high flow season samples.

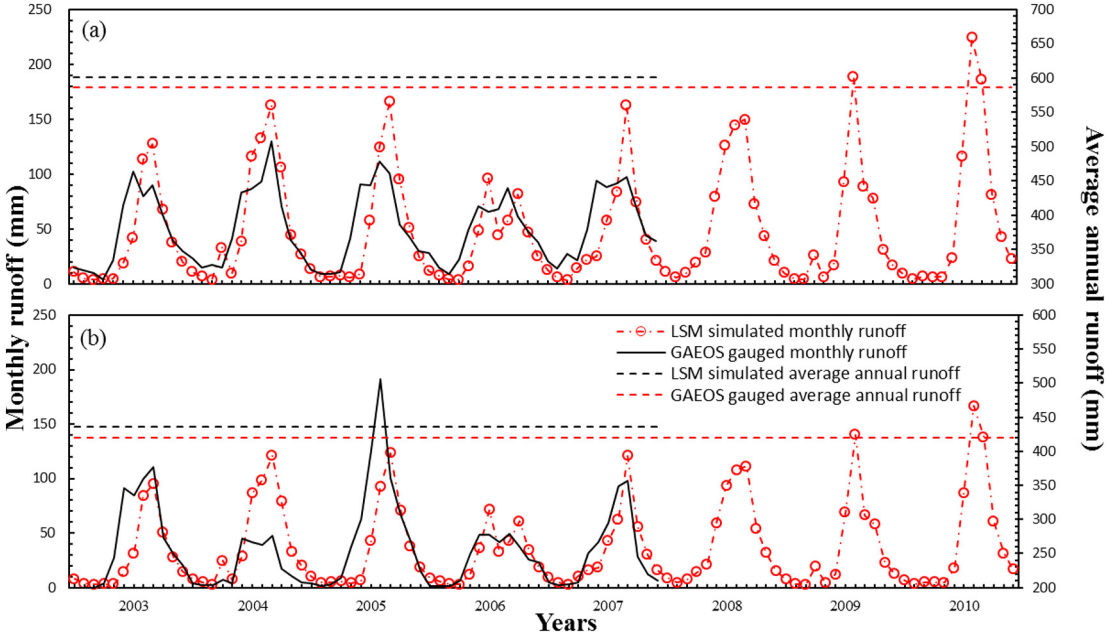

Fig. 4. The LSM model simulated and the GAEOS gauge-observed monthly and annual average runoff for WY-1 (a) and WY-13 (b).

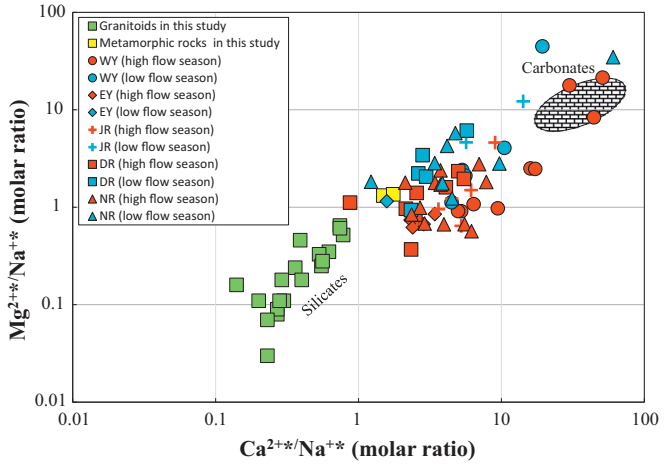

Fig. 5. Mixing diagrams using Na^+*-normalized molar ratios in the dissolved loads of the streams. Silicate end-members are from the elemental compositions of the fresh silicate rocks in the studied area. Carbonate end-member is from Gaillardet et al. (1999). * means the values are corrected for precipitation, glacier meltwater and hot spring water inputs.

$Na)_{sil}$ = 0.24 ± 0.12 were assigned to the silicate end-member by Gaillardet et al. (1999). Elemental ratios of silicate end-member were well documented for large river basins in Tibetan Plateau (e.g., $(Ca/Na)_{sil}$ = 0.7 ± 0.3 and $(Mg/Na)_{sil}$ = 0.3 ± 0.2, Krishnaswami et al., 1999; $(Ca/Na)_{sil}$ = 0.18–0.3, Galy and France-Lanord, 1999; $(Ca/Na)_{sil}$ = 0.17–0.58, Wu et al., 2008; $(Ca/Na)_{sil}$ = 0.25–0.31, Wang et al., 2016; $(Ca/Na)_{sil}$ = 0.54 and $(Mg/Na)_{sil}$ = 0.26, Yoon et al., 2008; $(Ca/Na)_{sil}$ = 0.2–0.5 and $(Mg/Na)_{sil}$ = 0.12–0.36, Wu, 2016). The Ca/Na and Mg/Na molar ratios measured in the bulk bedrocks of the studied area (Table 4) are within the range of the previous studies in the Tibetan Plateau. Mixing diagrams using the Na^+*-normalized molar ratios of stream waters are plotted in Fig. 5. Ca/Na = 50 ± 20 and Mg/Na = 10 ± 4 are adopted as the carbonate end-member (Gaillardet et al., 1999). Good relationships are observed between Mg^{2+}*/Na^+* and Ca^{2+}*/Na^+* molar ratios. The distribution of the samples in the plot shows a mixing trend between carbonate and silicate weathering. In this study, $(Ca/Na)_{sil}$ = 0.42 and $(Mg/Na)_{sil}$ = 0.25 are assigned to the silicate end-member (Table 4). The $(Ca/Na)_{sil}$ and $(Mg/Na)_{sil}$ for the streams draining metamorphic rocks could be higher for the existence of the schists. Besides, the preferential leaching of Ca^{2+} and Mg^{2+} could lead to high $(Ca/Na)_{sil}$ and $(Mg/Na)_{sil}$ ratios for stream waters draining granitoids (Millot et al., 2002). It is plausible that $(Ca/Na)_{sil}$ and $(Mg/Na)_{sil}$ of silicate end-member could be higher. Assigning an uncertainty of 50% for $(Ca/Na)_{sil}$ and $(Mg/Na)_{sil}$ as other authors did (Galy and France-Lanord, 1999; Krishnaswami et al., 1999; Gaillardet et al., 1999; Singh et al., 2005), the uncertainty of silicate weathering contribution could be 3%–26%. The contributions from carbonate weathering are estimated by deducting the precipitation, spring, glacier and silicate contributions from the total dissolved $[Ca^{2+}]$ and $[Mg^{2+}]$ in the streams.

5.2.3. *Contributions of the different sources*

The calculated contributions of K^+, Na^+, Ca^{2+}, Mg^{2+} and HCO_3^- (in eq) from different sources are given in Appendix A. The proportional contributions (%) of the major reservoirs to the total dissolved cation load (K^+, Na^+, Ca^{2+}, and Mg^{2+}, in eq) are illustrated in Fig. 6. Overall, the dissolved cation loads are dominated by rock weathering, which accounts for ~90% of the total dissolved cations for most streams. Silicates weathering accounts for 1.8–41.5% (averaging at 15.9%) of the total dissolved cations in high flow season and 0.04–33.1% (averaging at 9.5%) in low flow season. High silicate weathering contributions are observed for the granitic small catchments, especially for those at lower elevations (e.g., small catchments of DR), which may be attributed to the longer residence time of water in the sub-mountain environments. Longer residence time would favor greater relative inputs from weathering of silicates (Meybeck, 1987; White et al., 1999). Carbonate weathering accounts for 54.0–94.9% (averaging at 75.2%) of the total dissolved cations in high flow season and 49.1–96.1% (averaging at 77.2%) in low flow season. The glacier meltwater inputs are insignificant, generally < 1.5%. The precipitation contributes about 2.7% of the total cations on average. The contributions of hot spring water account for 7.7% of the total dissolved cations on average (mostly < 5%). The high ions concentrations of spring water (2–3 orders of magnitude higher than the stream water) make its contributions to dissolved loads disproportionately higher compared with its discharge contributions to stream runoff.

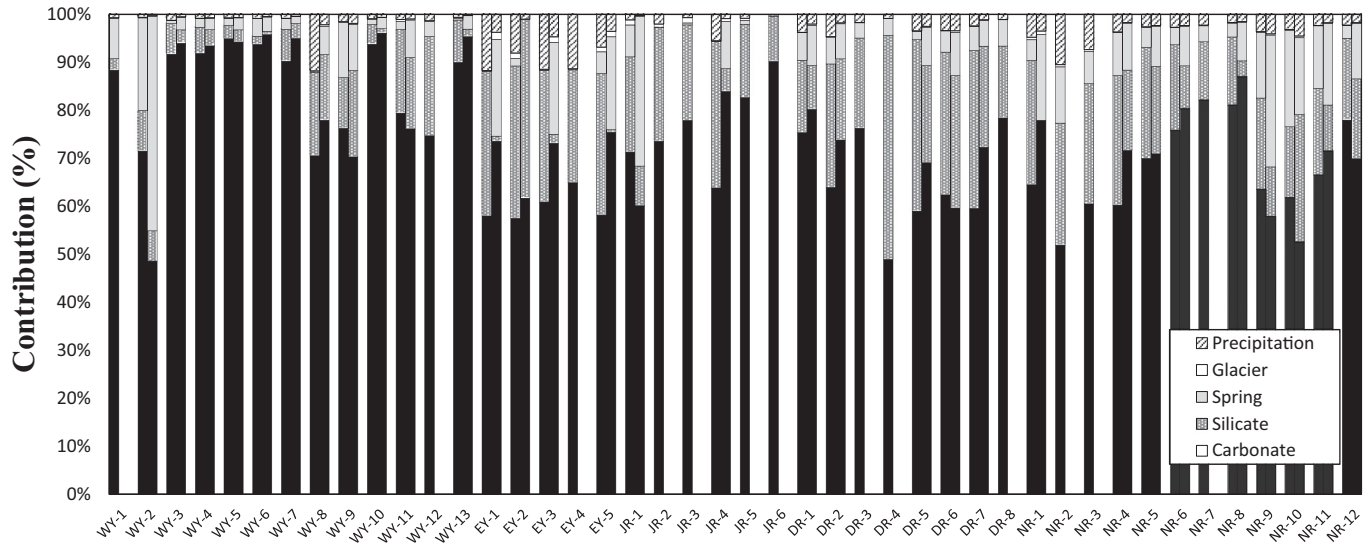

Fig. 6. Diagram showing the proportional contributions of each reservoir to the dissolved cation loads (K^+, Na^+, Ca^{2+} and Mg^{2+}, in eq) of stream waters in high flow season (left bar for a specific sample) and low flow season (right bar for a specific sample). All the streams were collected for high flow season samples, but some of them lack low flow season samples due to the absence of flow. The samples with only one bar are for high flow season samples.

5.3. Chemical weathering rates

The silicate cation weathering rate (SCWR), total cation weathering rate (TCWR), SiO_2 weathering rate (SiO_2-WR) and total chemical weathering rate (CWR) of the small catchments on the southeastern Tibetan Plateau are calculated based on the dissolved solid concentrations derived from chemical weathering in high flow and low flow seasons and the corresponding runoff. TCWR is the total cation flux ($Ca^{2+} + Mg^{2+} + Na^+ + K^+$) from chemical weathering, while the SCWR is the silicate-derived cation flux. CWR is the total mass of material flux by silicate and carbonate chemical weathering. The weathering rates are calculated as follows (West et al., 2005):

$$TCWR = {K^+}_{weath} + {Na^+}_{weath} + {Ca^{2+}}_{weath} + {Mg^{2+}}_{weath} \quad (12)$$

$$SiO_2 - WR = SiO_{2weath} \quad (13)$$

$$SCWR = {K^+}_{sil} + {Na^+}_{sil} + {Ca^{2+}}_{sil} + {Mg^{2+}}_{sil} \quad (14)$$

$$CWR = CaO_{weath} + MgO_{weath} + Na_2O_{weath} + K_2O_{weath} + SiO_{2weath} + CO_{2carb} \quad (15)$$

The subscript weath stands for chemical weathering flux of each element, sil stands for elements flux during silicate weathering, CO_{2carb} reflects the carbon lost in the weathering of carbonate, calculated based on a molar 1:1 ratio with the $Ca^{2+} + Mg^{2+}$ from carbonate weathering. Physical erosion rates are calculated based on SPM contents in different seasons and the corresponding runoff as previous studies did (Edmond et al., 1995; Louvat and Allègre, 1997; Gaillardet et al., 1999; Picouet et al., 2002; Moon et al., 2007). The physical erosion rates are probably underestimations of the real value, because the fluxes of sediments as riverbed sands and the influence of flood and landslide events are not considered. Total denudation rates (TDR) are calculated as the sum of physical erosion rate plus the calculated CWR. A few streams dried up in low flow season and the weathering rates of these catchments are not calculated here. The seasonal and annual weathering rates (in $t/km^2/yr$) are presented in Table 5.

The SiO_2-WR, TCWR, CWR and TDR range from 2.3 to 15.5 (averaging at 4.9), 2.2 to 26.0 (averaging at 11.1), 8.4 to 74.9 (averaging at 32.6) and 8.9 to 1907.9 (averaging at 139.8) $t/km^2/yr$, respectively. The main uncertainties in the rock weathering rate estimation arise from uncertainties on discharge and variations of chemical and isotopic compositions of end-members. For the calculation of TCWR, SiO_2-WR and CWR, the propagated uncertainty is about 21% from the uncertainty on the water mixing calculations (averaging at 20%) and the uncertainty on the runoff estimation (~4%). The CWR and TDR of the small catchments in high flow season are 4 and 18 times of those in low flow season, respectively, which may be attributed to the higher temperature and runoff in high flow season. Spatially, the TDR are much higher in glacial catchments (e.g., small catchments of WY and JR), resulting from glacial erosion. Assuming that the density of rock is 2.7 g/cm^3 (Galy and France-Lanord, 1999), the total denudation rates of the small catchments are calculated at 3.3–706.6 mm/kyr (Table 5). The rates are comparable to the TDR in the Tibetan Plateau deduced from cosmogenic ^{10}Be concentrations: 3–2100 mm/kyr (Lal et al., 2004), but lower than the total denudation rates in the eastern syntaxis (~10,000 mm/kyr, Burg et al., 1998) and western syntaxis (3000–5000 mm/kyr, Moore and England, 2001) of the Himalayas.

The SCWR averages at 2.0 (0.6–4.0), 4.6 (4.0–5.2), 0.8 (0.7–0.9), 1.8 (0.9–3.0) and 1.5 (1.0–1.9) $t/km^2/yr$ for the small catchments of WY, JR, EY, DR and NR, respectively (Table 5). The area-weighted mean SCWR of the small catchments are 1.8 (0.6–5.2) $t/km^2/yr$. The propagated uncertainty for SCWR is about 29% from the uncertainty on the water mixing calculations and the pre-assigned $(Ca/Na)_{sil}$ and $(Mg/Na)_{sil}$ ratios (averaging at 28%), and the uncertainty on the runoff (~4%).

The SCWR are significantly variable from one catchment to another, which are controlled by many factors, e.g., lithology, climate (rainfall, runoff and temperature), topography, physical denudation rates, etc. The SCWR of the small catchments and other catchments documented in previous studies are plotted in terms of SCWR versus runoff and MAT (Fig. 7). In the first place, lithology should have a strong effect on weathering rates (Bluth and Kump, 1994). The SCWR in this study are lower than those of basaltic catchments with similar temperature and runoff, such as Kamchatka Peninsula (~8 $t/km^2/yr$) and Massif Central (~5.6 $t/km^2/yr$) (Négrel and Deschamps, 1996; Dessert et al., 2003, 2009) (Fig. 7). According to Dessert et al. (2001) the chemical weathering rate of volcanic rock is 5–10 times higher than the chemical weathering of granite and gneiss. With similar or even lower runoff and MAT, the metamorphic catchments generally have higher SCWR than those of the granitic catchments (e.g., WY-4 and WY-7 are higher than NR-6 and NR-9, Fig. 7), which is attributed to the difference in the weathering resistance of granitoids and the metamorphic rocks (e.g., schist and slate). In granitic environments, chemical weathering is

Table 5
Weathering rates and total denudation rates of the small catchments on the southeastern Tibetan Plateau, China.

Catchment No.	SCWR[a]			TCWR			SiO_2-WR			CWR			TDR			TDR[b]
	High flow season	Low flow season	Total	High flow season	Low flow season	Total	High flow season	Low flow season	Total	High flow season	Low flow season	Total	High flow season	Low flow season	Total	
	$t/km^2/yr$			$t/km^2/yr$			$t/km^2/yr$			$t/km^2/yr$			$t/km^2/yr$			mm/kyr
Glacial catchments (partial glacial cover)																
West bank of Yajiahe River																
WY-2	3.2	0.7	4.0	21.4	4.6	26.0	6.3	3.9	10.2	58.1	15.3	73.4	109.9	15.4	125.4	46.4
WY-3	1.9	0.2	2.1	17.9	3.5	21.4	2.2	0.4	2.6	46.3	9.5	55.8	47.8	9.6	57.3	21.2
WY-4	2.1	0.2	2.3	19.3	3.3	22.6	2.4	0.4	2.8	50.0	9.0	58.9	53.7	9.1	62.7	23.2
WY-5	1.2	0.2	1.4	21.0	3.8	24.8	2.0	0.4	2.5	54.6	10.3	64.9	57.3	10.4	67.7	25.1
WY-6	0.7	0.1	0.7	15.7	3.7	19.4	2.3	0.4	2.7	45.0	11.5	56.5	1895.9	12.0	1907.9	706.6
WY-7	2.2	0.3	2.6	17.8	5.3	23.2	2.4	0.4	2.8	47.6	16.3	63.9	378.0	16.4	394.4	146.1
WY-8	0.4	0.2	0.6	1.8	1.3	3.1	1.7	1.4	3.1	5.9	4.6	10.6	36.5	4.6	41.1	15.2
WY-9	1.2	0.3	1.6	9.0	1.4	10.4	4.0	0.8	4.8	25.8	4.1	29.9	25.9	4.2	30.1	11.1
WY-10	1.0	0.1	1.1	14.9	3.5	18.4	2.1	0.4	2.5	42.0	10.5	52.5	285.7	10.5	296.2	109.7
WY-11	3.1	0.7	3.9	14.5	3.8	18.3	6.1	1.6	7.6	40.4	11.0	51.4	627.0	11.1	638.1	236.3
WY-13	1.8	0.2	2.0	14.8	4.7	19.4	1.9	0.4	2.3	37.9	12.6	50.5	39.1	13.0	52.1	19.3
Jiazela River																
JR-1	3.7	1.5	5.2	14.7	9.4	24.0	12.0	3.5	15.5	46.7	28.3	74.9	53.3	28.4	81.6	30.2
JR-4	3.8	0.2	4.0	10.2	2.6	12.8	9.7	2.3	12.0	33.6	9.5	43.1	34.1	9.6	43.6	16.2
Sub-Montane Catchments (soil mantled)																
East bank of Yajiahe River																
EY-1	0.9	0.0	0.9	2.5	0.4	3.0	3.7	0.9	4.6	9.5	2.0	11.5	9.9	2.1	11.9	4.4
EY-2	0.7	0.2	0.9	1.9	0.5	2.3	2.9	0.8	3.6	7.1	1.8	8.9	7.7	1.8	9.6	3.5
EY-3	0.6	0.0	0.7	1.9	0.4	2.2	2.4	0.7	3.1	6.7	1.6	8.4	7.2	1.6	8.9	3.3
EY-5	0.8	0.0	0.8	2.2	0.4	2.5	3.5	1.1	4.6	8.5	2.2	10.7	11.9	2.2	14.1	5.2
Daduhe River																
DR-1	0.7	0.1	0.9	3.7	0.9	4.6	2.4	0.5	2.9	11.6	2.9	14.6	13.9	2.9	16.8	6.2
DR-2	1.0	0.3	1.3	3.0	1.1	4.0	2.8	0.7	3.5	9.8	3.5	13.3	67.0	3.5	70.6	26.1
DR-5	1.8	0.2	2.0	4.6	0.7	5.3	4.1	0.7	4.8	14.1	2.4	16.5	14.2	2.5	16.7	6.2
DR-7	2.5	0.4	3.0	6.2	1.7	7.9	4.9	0.7	5.6	19.0	4.9	23.8	32.8	5.2	38.0	14.1
Nanyahe River																
NR-1	1.0	0.0	1.0	3.2	0.5	3.7	3.6	0.7	4.3	11.1	2.1	13.2	11.3	2.3	13.5	5.0
NR-4	1.4	0.3	1.7	4.0	1.4	5.4	4.3	0.9	5.2	13.3	4.6	17.9	14.6	4.9	19.5	7.2
NR-5	1.6	0.3	1.9	6.0	1.1	7.1	3.8	0.7	4.5	17.8	3.3	21.2	19.1	3.4	22.4	8.3
NR-6	1.3	0.1	1.4	6.0	1.1	7.1	3.7	0.7	4.4	17.9	3.3	21.3	19.1	3.4	22.5	8.3
NR-8	1.8	0.1	1.9	9.5	1.6	11.0	3.7	0.6	4.3	26.5	4.7	31.3	27.3	17.5	44.9	16.6
NR-9	1.0	0.1	1.1	3.6	0.5	4.1	4.2	1.0	5.2	12.9	2.3	15.2	13.4	2.3	15.7	5.8
NR-10	0.9	0.2	1.1	3.7	0.4	4.1	4.2	0.9	5.1	13.5	2.0	15.5	14.6	2.1	16.7	6.2
NR-11	1.4	0.2	1.6	5.8	1.1	6.9	4.3	0.8	5.1	18.4	3.9	22.3	19.1	3.9	23.1	8.5
NR-12	1.4	0.3	1.7	7.4	1.4	8.8	3.8	0.8	4.5	21.1	4.1	25.3	27.2	4.2	31.4	11.6

[a] SCWR = silicate cation weathering rate; TCWR = total cation weathering rate; SiO_2-WR = SiO_2 weathering rate; CWR = total chemical weathering rate; TDR = physical erosion rate + total chemical weathering rate.
[b] Conversed from the TDR in $t/km^2/yr$ by assuming the density of rock is 2.7 g/cm^3.

dominated by the more easily weathering minerals (Sverdrup and Warfvinge, 1995), e.g., biotite, amphibole, plagioclase, epidote, and apatite. The relative reactivity of minerals decreases in the order: mafic silicates > feldspars > quartz (White and Blum, 1995). The small catchments in this study have non-uniform granitoids lithologies as we discussed in Sections 2 and 4.3, while the climatic conditions are found to be similar for some of the small catchments, therefore hold potential to explore the lithological control of silicate weathering rate in the granitic environment. The comparison between the granitic small catchments demonstrated that with similar MAT and runoff, the SCWR of the small catchments of WY draining biotite granites are generally higher than those of NR and EY draining granites and plagiogranites (e.g., WY-13 is higher than NR-1 and the catchments of EY, Fig. 7), which may be attributed to the relatively enrichment of easily weathering biotite in the bedrocks (Table 4). The NR-4, NR-8 and DR-7 with diorite exposure (Fig. 1) have relatively higher SCWR than other granitic catchments (e.g., DR-1-2 and NR-9-10, Fig. 7) as a result of the abundant amphibole in the bedrocks.

The SCWR of the small catchments in this study are higher than those with low temperature and runoff, such as the Heihe, Shiyang, Shule, Niya and Hetian river basins on the northern Tibetan Plateau, and the river basins in the Siberia and Canada (Wu, 2016; Millot et al., 2002; West et al., 2005). Whereas they are lower than those on the southern slope of Tibetan Plateau (e.g., Ganges, Galy and France-Lanord, 1999), and Puerto Rico and Cote d'ivoire (West et al., 2005), where is with high temperature and/or runoff (Fig. 7). The SCWR of the small catchments are comparable with the upper reaches of the river basins on the eastern Tibetan Plateau (e.g., the Yellow, Changjiang, Mekong, Salween and Brahmaputra) and granitic catchments with similar temperature and runoff in mountainous areas (Wu et al., 2005; Wu et al., 2008; Chetelat et al., 2008; Noh et al., 2009; Hren et al., 2007; Millot et al., 2002; West et al., 2005) (Fig. 7). Moreover, compared with tropical arid regions (e.g., the Niger and Zambezi) and cold regions with abundant runoff (e.g., the Karelia, Kola and Svalbard), the studied catchments have higher SCWR (Gaillardet et al., 1999; Picouet et al., 2002; Hodson et al., 2000; Zakharova et al., 2007) (Fig. 7). The average SCWR of the small catchments is about 6 times higher in high flow season (1.6 $t/km^2/yr$) than in low flow season (0.3 $t/km^2/yr$), which could be attributed to both higher temperature and runoff in high flow season. Therefore, both high temperature and runoff are essential for high SCWR (White and Blum, 1995; Oliva et al., 2003; Gurumurthy et al., 2012; Maher and Chamberlain, 2014; Fernandes

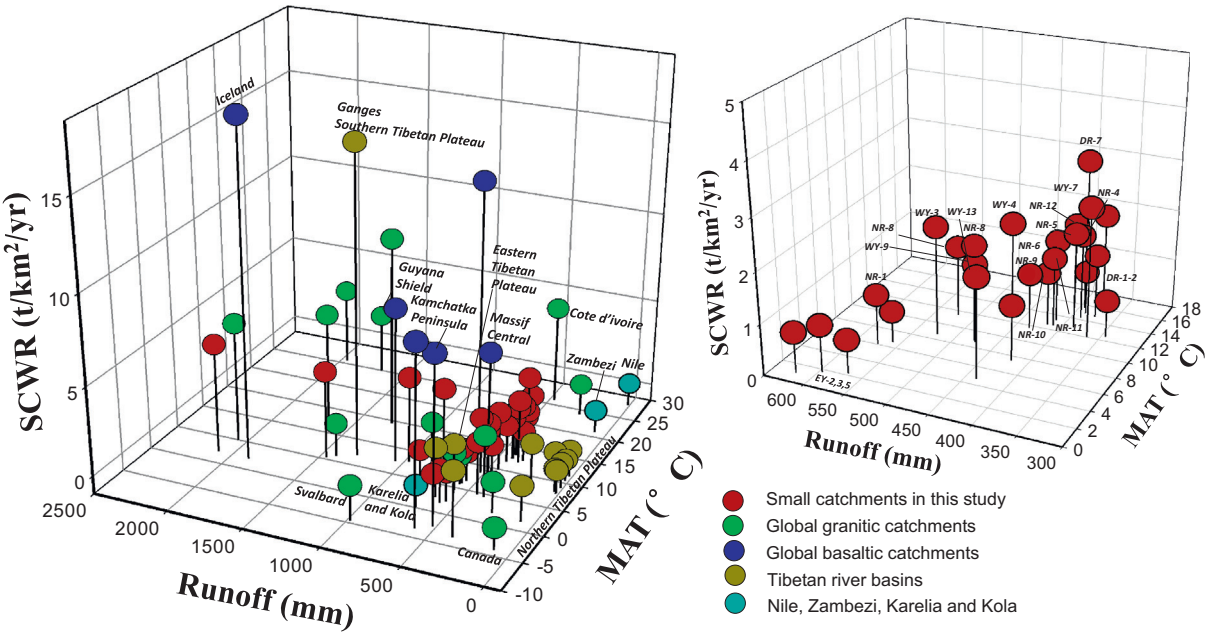

Fig. 7. Comparison of SCWR with temperature and runoff for the small catchments in this study, global small silicate catchments (Millot et al., 2002; Oliva et al., 2003; West et al., 2005 and Fernandes et al., 2016 and references therein), basaltic catchments (Négrel and Deschamps, 1996; Dessert et al., 2003, 2009 and references therein), Tibetan catchments (Noh et al., 2009; Wu et al., 2005, 2008; Wu, 2016 and references therein) and world river basins (calculated from Gaillardet et al., 1999; Picouet et al., 2002; Zakharova et al., 2007). This plot confirms that the highest silicate fluxes result from the combination of high runoff and warm temperature as observed by White and Blum (1995) and Oliva et al. (2003).

et al., 2016).

However, hot and humid climates do not necessarily generate high silicate weathering rates (Millot et al., 2002; Oliva et al., 2003; West et al., 2005; Braun et al., 2005). With much lower runoff and MAT, some of the studied small catchments have similar SCWR to those of British Columbia (2.5 t/km^2/yr, West et al., 2005) and the Guyana Shield (2.4 t/km^2/yr, Edmond et al., 1995) (Figs. 7 and 8), which indicates that climate factors are insufficient to explain the weathering rates. The relationship between the SCWR and TDR are shown in Fig. 8. The positive relationship supports the view that physical erosion

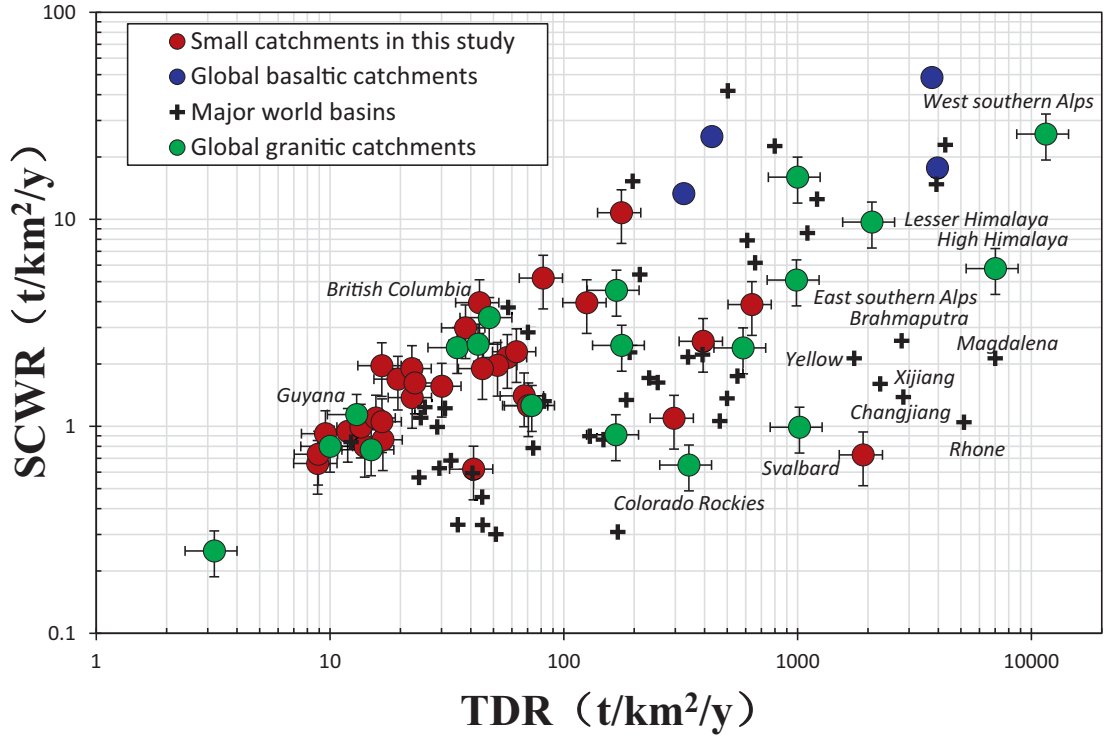

Fig. 8. The SCWR of the small catchments compared with worldwide small catchments and large river basins on the basis of SCWR versus TDR. Granitic small catchments (Millot et al., 2002; Oliva et al., 2003; West et al., 2005; Fernandes et al., 2016 and references therein) basaltic catchments (Dessert et al., 2003, 2009 and references therein) and major word basins, including Tibetan river basins (calculated from Gaillardet et al., 1999) are also plotted for comparison.

processes of orogenic zone, the Tibetan Plateau especially, play a key role in continental chemical weathering (Raymo et al., 1988; Raymo and Ruddiman, 1992; Larsen et al., 2014). The low SCWR accompanied with low TDR of the catchments of EY, may be resulted from insufficient fresh materials supply by erosion. Some SCWR exhibit no clear relationship with TDR, especially in the catchments with extremely high TDR (Fig. 8), which may be attributed to the "weathering-limited" regimes. In these cases, weathering rates are dependent on the kinetics of the reactions regulated by climatic factors, such as MAT and runoff (Stallard and Edmond, 1983; West et al., 2005).

6. Conclusions

This paper presents the hydro-geochemical investigations of 44 small catchments on the southeastern Tibetan Plateau. The Noah LSM model is applied to obtain the annual runoff of the catchments. The hydrograph separation and the chemical mass balance methods are jointly used to investigate the hydro-geochemical processes and quantify the contributions of dissolved solids from different sources. The dissolved solids are from five major reservoirs (carbonates, silicates, precipitation, glacier and spring). The contributions of rock weathering account for ~90% of the total dissolved cations. Silicates weathering accounts for on average 15.9% and 9.5% of the total dissolved cations in high and low flow season, respectively. The SiO_2-WR, TCWR, CWR and TDR range from 2.3 to 15.5, 2.2 to 26.0, 8.4 to 74.9 and 8.9 to 1907.9 t/km^2/yr, respectively. The SCWR range from 0.6 to 5.2 t/km^2/yr, and the area-weighted mean SCWR of the small catchments is 1.8 t/km^2/yr. The comparisons between the small catchments and with other catchments indicate that lithology, climate (temperature and runoff) and physical erosion are the parameters controlling chemical weathering. Under the similar lithological settings, high SCWR are observed for the small catchments with high MAT and runoff. Meanwhile, the positive relationship between SCWR and TDR supports the view that physical erosion processes of Tibetan Plateau play a key role in chemical weathering. Further exploration on detailed aspects on controlling factors of weathering mechanisms and rates would provide more information for silicate weathering under various climatic and tectonic conditions.

Supplementary data to this article can be found online at https://doi.org/10.1016/j.chemgeo.2018.09.030.

Acknowledgments

The authors appreciate the insightful comments and constructive suggestions from the editor and the anonymous reviewers. This work was financially supported by the Strategic Priority Research Program of Chinese Academy of Sciences (grant Nos. XDB26000000 and XDB15010405), and Natural Science Foundation of China (grant Nos. 41673020, 91747202, 41772380 and 41730857).

References

Berner, R.A., 1991. A model for atmospheric CO_2 over Phanerozoic time. Am. J. Sci. 291, 339–376.
Berner, R.A., Lassaga, A.C., Garrels, R.M., 1983. The carbonate-silicate geochemical cycle and its effect on atmospheric carbon dioxide over the past 100 million years. Am. J. Sci. 283, 641–683.
Blum, J.D., Gazis, C.A., Jacobson, A.D., Chamberlain, C.P., 1998. Carbonate versus silicate weathering in the Raikhot watershed within the high Himalayan crystalline series. Geology 26, 411–414.
Bluth, G., Kump, L., 1994. Lithologic and climatologic controls of river chemistry. Geochim. Cosmochim. Acta 58, 2341–2359.
Braun, J.J., Ngoupayou, J.R.N., Viers, J., Dupré, B., Bedimo, J.P.B., Boeglin, J.L., Robain, H., Nyeck, B., Freydier, R., Nkamdjou, L.S., Rouiller, J., Muller, J.P., 2005. Present weathering rates in a humid tropical watershed: Nsimi, South Cameroon. Geochim. Cosmochim. Acta 69, 357–387.
Burg, J.-P., Nievergelt, P., Oberli, F., Seward, D., Davy, P., Maurin, J.-C., Diao, Z., Meier, M., 1998. The Namche Barwa syntaxis: evidence for exhumation related to compressional crustal folding. J. Asian Earth Sci. 16 (2–3), 239–252.
Buttle, J.M., 1994. Isotope hydrograph separations and rapid delivery of pre-event water from drainage basins. Prog. Phys. Geogr. 18, 16–41.
Cartwright, I., Hoffmann, H., Sirianos, M., Weaver, T.R., Simmons, G.T., 2011. Geochemical and ^{222}Rn constraints on baseflow to the Murray River, Australia, and timescales for the decay of low-salinity groundwater lenses. J. Hydrol. 405, 333–343.
Chetelat, B., Liu, C.-Q., Zhao, Z.Q., Wang, Q.L., Li, S.-L., Li, J., Wang, B.L., 2008. Geochemistry of the dissolved load of the Changjiang Basin rivers: anthropogenic impacts and chemical weathering. Geochim. Cosmochim. Acta 72, 4254–4277.
Clark, I.D., Fritz, P., 1997. Environmental Isotopes in Hydrogeology. Lewis Publisher, Boca Raton, FL, USA, pp. 328.
Dalai, T.K., Krishnaswami, S., Sarin, M.M., 2002. Major ion chemistry in the headwaters of the Yamuna river system: chemical weathering its temperature dependence and CO_2 consumption in the Himalaya. Geochim. Cosmochim. Acta 63, 3397–3416.
Das, P., Sarma, K.P., Jha, P.K., Ranjan, R., Herbert, R., Kumar, M., 2016. Understanding the cyclicity of chemical weathering and associated CO_2, consumption in the Brahmaputra River basin (India): the role of major rivers in climate change mitigation perspective. Aquat. Geochem. 22 (3), 225–251.
Dessert, C., Dupré, B., François, L.M., Schott, J., Gaillardet, J., Chakrapani, G.J., Bajpai, S., 2001. Erosion of Deccan Traps determined by river geochemistry: impact on the global climate and the $^{87}Sr/^{86}Sr$ ratio of seawater. Earth Planet. Sci. Lett. 188, 459–474.
Dessert, C., Dupré, B., Gaillardet, J., François, L.M., Allègre, C.J., 2003. Basalt weathering laws and the impact of basalt weathering on the global carbon cycle. Chem. Geol. 202 (3), 257–273.
Dessert, C., Gaillardet, J., Dupre, B., Schott, J., Pokrovsky, O.S., 2009. Fluxes of high- versus low-temperature water-rock interactions in aerial volcanic areas: example from the Kamchatka Peninsula, Russia. Geochim. Cosmochim. Acta 73 (1), 148–169.
Edmond, J.M., Palmer, M.R., Measures, C.I., Grant, B., Stallard, R.F., 1995. The fluvial geochemistry and denudation rate of the Guayana Shield in Venezuela, Colombia, and Brazil. Geochim. Cosmochim. Acta 59 (16), 3301–3325.
Fernandes, A.M., Conceição, F.T.D., Junior, E.P.S., Sardinha, D.S., Mortatti, J., 2016. Chemical weathering rates and atmospheric/soil CO_2, consumption of igneous and metamorphic rocks under tropical climate in southeastern Brazil. Chem. Geol. 443, 54–66.
Gabet, E.J., Wolff-Boenisch, D., Langner, H., Burbank, D., Putkonen, J., 2010. Geomorphic and climatic controls on chemical weathering in the High Himalayas of Nepal. Geomorphology 122, 205–210.
Gaillardet, J., Galy, A., 2008. Himalaya, carbon sink or source? Science 320, 1727–1728.
Gaillardet, J., Dupré, B., Allégre, C.J., Négrel, P., 1997. Chemical and physical denudation in the Amazon River Basin. Chem. Geol. 142, 141–173.
Gaillardet, J., Dupré, B., Louvat, P., Allègre, C.J., 1999. Global silicate weathering and CO_2 consumption rates deduces from the chemistry of large rivers. Chem. Geol. 159, 3–30.
Galy, A., France-Lanord, C., 1999. Weathering processes in the Ganges-Brahmaputra basin and the riverine alkalinity budget. Chem. Geol. 159, 31–60.
Garrels, R.M., Mackenzie, F.T., 1967. Origin of the chemical compositions of some springs and lakes. In: Gould, R.F. (Ed.), Equilibrium Concepts in Natural Water Systems: Advances in Chemistry Series. vol. 67. American Chemical Society, Washington DC, pp. 222–242.
Gurumurthy, G.P., Balakrishna, K., Riotte, J., Braun, J.J., Audry, S., Shankar, H.N.U., Manjunatha, B.R., 2012. Controls on intense silicate weathering in a tropical river, southwestern India. Chem. Geol. 300-301, 61–69.
Hagedorn, B., Whittier, R.B., 2015. Solute sources and water mixing in a flashy mountainous stream (Pahsimeroi River, U.S. Rocky Mountains): implications on chemical weathering rate and groundwater-surface water interaction. Chem. Geol. 391, 123–137.
Hindshaw, R.S., Tipper, E.T., Reynolds, B.C., Lemarchand, E., Wiederhold, J.G., Magnusson, J., Bernasconi, S.M., Kretzschmar, R., Bourdon, B., 2011. Hydrological control of stream water chemistry in a glacial catchment (Damma Glacier, Switzerland). Chem. Geol. 285 (1–4), 215–230.
Hodson, A., Tranter, M., Vatne, G., 2000. Contemporary rates of chemical denudation and atmospheric CO_2 sequestration in glacier basins: an Arctic perspective. Earth Surf. Process. Landf. 25, 1447–1471.
Hosein, R., Arn, K., Steinmann, P., Adatte, T., Föllmi, K.B., 2004. Carbonate and silicate weathering in two presently glaciated, crystalline catchments in the Swiss Alps. Geochim. Cosmochim. Acta 68, 1021–1033.
Hren, M.T., Chamberlain, C.P., Hilley, G.E., Blisniuk, P.M., Bookhagen, B., 2007. Major ion chemistry of the Yarlung Tsangpo-Brahmaputra River: chemical weathering, erosion, and CO_2 consumption in the southern Tibetan plateau and eastern Syntaxis of the Himalaya. Geochim. Cosmochim. Acta 71, 2907–2935.
Huh, Y.S., 2003. Chemical weathering and climate—a global experiment: a review. Geosci. J. 7, 277–288.
Jacobson, A.D., Blum, J.D., Walter, L.M., 2002. Reconciling the elemental and Sr isotope composition of Himalayan weathering fluxes: insights from the carbonate geochemistry of stream waters. Geochim. Cosmochim. Acta 66, 3417–3429.
Johannessen, M., Henriksen, A., 1978. Chemistry of snow meltwater: changes in concentration during melting. Water Resour. Res. 14, 615–619.
Kasting, J., 1987. Theoretical constraints on oxygen and carbon dioxide concentrations in the Precambrian atmosphere. Precambrian Res. 34, 205–229.
Krishnaswami, S., Singh, S.K., Dalai, T.K., 1999. Silicate weathering in the Himalaya: role in contributing to major ions and radiogenic Sr to the Bay of Bengal. In: Ocean Science, Trends and Future Directions, pp. 23–51.
Ladouche, B., Probst, A., Viville, D., Idir, S., Baqué, D., Loubet, M., 2001. Hydrograph separation using isotopic, chemical and hydrological approaches (Strengbach catchment, France). J. Hydrol. 242 (3–4), 255–274.
Lal, D., Harris, N.B.W., Sharma, K.K., Ding, L., Gu, L., Dong, W., Jull, A.J.T., 2004. Erosion history of the Tibetan Plateau since the last interglacial: constraints from the first studies of cosmogenic ^{10}Be from Tibetan bedrock. Earth Planet. Sci. Lett. 217 (1–2), 33–42.
Larsen, I.J., Almond, P.C., Eger, A., Stone, J.O., Montgomery, D.R., Malcolm, B., 2014. Rapid soil production and weathering in the Southern Alps, New Zealand. Science 343 (6171), 637.

Li, J., Su, Z., 1996. Glaciers in the Hengduan Mountains. Science Press, Beijing, pp. 1–110 (In Chinese).
Li, W., Cheng, G., Luo, J., Lu, R., Liao, X., 2004. Features of the natural runoff of Hailuo Ravine in Mt. Gongga. J. Mt. Sci. 22 (6), 697–701 (in Chinese with English abstract).
Li, S.-L., Chetelat, B., Yue, F., Zhao, Z., Liu, C.-Q., 2014a. Chemical weathering processes in the Yalong River draining the eastern Tibetan Plateau, China. J. Asian Earth Sci. 88, 74–84.
Li, Z., Feng, Q., Liu, W., Wang, T., Cheng, A., Gao, Y., G., X., P., Y., 2014b. Study on the contribution of cryosphere to runoff in the cold alpine basin: a case study of Hulugou River Basin in the Qilian Mountains. Glob. Planet. Chang. 122 (345–361), 345–361.
Li, S., Xia, X., Zhou, B., Zhang, S., Zhang, L., Mou, X., 2018. Chemical balance of the Yellow River source region, the northeastern Qinghai-Tibetan Plateau: Insights about critical zone reactivity. Appl. Geochem. 90, 1–12.
Liu, F., Williams, M.W., Caine, N., 2004. Source waters and flow paths in an alpine catchment, Colorado Front Range, United States. Water Resour. Res. 40, W09401.
Liu, Y., Fan, N., An, S., Bai, X., Liu, F., Xu, Z., Wang, Z., Liu, S., 2008. Characteristics of water isotopes and hydrograph separation during the wet season in the Heishui River, China. J. Hydrol. 353, 314–321.
Liu, Q., Liu, S., Zhang, Y., Wang, X., Zhang, Y., Guo, W., Xu, J., 2010. Recent shrinkage and hydrological response of Hailuogou Glacier, a monsoon temperate glacier on the east slope of Mount Gongga, China. J. Glaciol. 56 (196), 215–224.
Louvat, P., Allègre, C.J., 1997. Present denudation rates on the island of Réunion determined by river geochemistry: basalt weathering and mass budget between chemical and mechanical erosions. Geochim. Cosmochim. Acta 61, 3645–3669.
Maher, K., Chamberlain, C.P., 2014. Hydrologic regulation of chemical weathering and the geologic carbon cycle. Science 343 (6178), 1502–1504.
Malard, F., Tockner, K., Ward, J.V., 1999. Shifting dominance of subcatchment water sources and flow paths in a glacial floodplain, Val Roseg, Switzerland. Arct. Antarct. Alp. Res. 31, 135–150.
Marsh, P., Pomeroy, J.W., 1999. Spatial and temporal variations in snowmelt runoff chemistry, Northwest Territories, Canada. Water Resour. Res. 35, 1559–1567.
McCallum, J.L., Cook, P.G., Brunner, P., Berhane, D., 2010. Solute dynamics during bank storage flows and implications for chemical base flow separation. Water Resour. Res. 46, 58–72.
Meybeck, M., 1987. Global chemical weathering of surficial rocks estimated from river dissolved loads. Am. J. Sci. 287, 401–428.
Meybeck, M., 2003. Treatise on Geochemistry, Surface and Ground Water, Weathering, and Soils. 5. Elsevier, Amsterdam, pp. 207–223.
Meyer, H., Strauss, H., Hetzel, R., 2009. The role of supergene sulphuric acid during weathering in small river catchments in low mountain ranges of Central Europe: implications for calculating the atmospheric CO_2 budget. Chem. Geol. 268, 41–51.
Millot, R., Gaillardet, J., Dupré, B., Allègre, C.J., 2002. The global control of silicate weathering rates and the coupling with physical erosion: new insights from rivers of the Canadian shield. Earth Planet. Sci. Lett. 196 (1), 83–98.
Moon, S., Huh, Y., Qin, J., Van Pho, N., 2007. Chemical weathering in the Hong Red River basin: rates of silicate weathering and their controlling factors. Geochim. Cosmochim. Acta 71, 1411–1430.
Moon, S., Chamberlain, C.P., Hilley, G.E., 2014. New estimates of silicate weathering rates and their uncertainties in global rivers. Geochim. Cosmochim. Acta 134 (2), 257–274.
Moore, M.A., England, P.C., 2001. On the inference of denudation rates from cooling ages of minerals. Earth Planet. Sci. Lett. 185 (3–4), 265–284.
Négrel, P., Deschamps, P., 1996. Natural and anthropogenic budgets of a small watershed in the massif central (France): chemical and strontium isotopic characterization of water and sediments. Aquat. Geochem. 2 (1), 1–27.
Négrel, P., Allègre, C.J., Dupé, B., Lewin, E., 1993. Erosion sources determined by inversion of major and trace element ratios and Sr isotopic ratios in river water. The Congo basin case. Earth Planet. Sci. Lett. 120, 59–76.
Niu, G.-Y., Yang, Z.-L., Mitchell, K.E., Chen, F., Ek, M.B., Barlage, M., Kumar, A., Manning, K., Niyogi, D., Rosero, E., Tewari, M., Xia, Y., 2011. The community Noah land surface model with multi-parameterization options (Noah-MP): 1. Model description and evaluation with local-scale measurements. J. Geophys. Res. 116, D12109.
Noh, H., Huh, Y., Qin, J., Ellis, A., 2009. Chemical weathering in the Three Rivers region of Eastern Tibet. Geochim. Cosmochim. Acta 73, 1857–1877.
Oliva, P., Viers, J., Dupré, B., 2003. Chemical weathering in granitic environments. Chem. Geol. 202, 225–256.
Picouet, C., Dupré, B., Orange, D., Valladon, M., 2002. Major and trace element geochemistry in the upper Niger River (Mali): physical and chemical weathering rates and CO_2 consumption. Chem. Geol. 185 (1–2), 93–124.
Pitman, A.J., 2003. The evolution of, and revolution in, land surface schemes designed for climate models. Int. J. Climatol. 23, 479–510.
Qin, J., Huh, Y., Edmond, J.M., Du, G., Ran, J., 2006. Chemical and physical weathering in the Min Jiang, a headwater tributary of the Yangtze River. Chem. Geol. 227, 53–69.
Raymo, M.E., Ruddiman, W.F., 1992. Tectonic forcing of late Cenozoic climate. Nature 359, 117–122.
Raymo, M.E., Ruddiman, W.F., Froelich, P.N., 1988. Influence of late Cenozoic mountain-building on ocean geochemical cycles. Geology 16, 649–653.
Regional Geological Archive of Gongga Region, Sichuan. Geological Bureau of Sichuan Province, China (in Chinese).
Regional Geological Archive of Shimian Region, Sichuan. Geological Bureau of Sichuan Province, China (in Chinese).
Regional Geological Archive of Yingjing Region, Sichuan. Geological Bureau of Sichuan Province, China (in Chinese).
Ruddiman, W.F. (Ed.), 1997. Tectonics, Uplift, and Climate Change. Plenum Publishing Co., New York, pp. 471–515.
Schulte, P., Geldern, R.V., Freitag, H., Karim, A., Négrel, P., Petelet-Giraud, E., Probst, A., Probst, J., Telmer, K., Veizer, J., Barth, J., 2011. Applications of stable water and carbon isotopes in watershed research: weathering, carbon cycling, and water balances. Earth-Sci. Rev. 109 (1), 20–31.
Sellers, P.J., Dickinson, R.E., Randall, D.A., Betts, A.K., Hall, F.G., Berry, J.A., Collatz, G.J., Denning, A.S., Moonky, H.A., Nobre, C.A., Sato, N., Field, C.B., Henderson-Sellers, A., 1997. Modeling the exchanges of energy, water, and carbon between continents and the atmosphere. Science 275 (5299), 502–509.
Shand, S.J., 1927. On the relations between silica, alumina, and the bases in eruptive rocks, considered as a means of classification. Geol. Mag. 64 (10), 446–449.
Singh, S.K., Sarin, M.M., France-Lanord, C., 2005. Chemical erosion in the eastern Himalaya: major ion composition of the Brahmaputra and $\delta^{13}C$ of dissolved inorganic carbon. Geochim. Cosmochim. Acta 69, 3573–3588.
Stallard, R.F., Edmond, J.M., 1983. Geochemistry of the Amazon: 2. The influence of geology and weathering environment on the dissolved-load. J. Geophys. Res. 88, 9671–9688.
Sverdrup, H., Warfvinge, P., 1995. Estimating field weathering rates using laboratory kinetics. Chemical weathering rates of silicate minerals. In: White, A.F., Brantley, S.L. (Eds.), Mineralogical Society of America. vol. 31. pp. 485–539.
Tipper, E.T., Bickle, M., Galy, A., West, A.J., Pomiés, C., Chapman, H.J., 2006. The short term climatic sensitivity of carbonate and silicate weathering fluxes: insight from seasonal variations in river chemistry. Geochim. Cosmochim. Acta 70, 2737–2754.
Turchyn, A.V., Tipper, E.T., Galy, A., Lo, J.K., Bickle, M.J., 2013. Isotope evidence for secondary sulfide precipitation along the Marsyandi River, Nepal, Himalayas. Earth Planet. Sci. Lett. 374 (4), 36–46.
Turner, J., Bradd, J., Waite, T., 1992. Conjunctive use of isotopic techniques to elucidate solute concentration and flow processes in dryland salinized catchments. In: Isotope Techniques in Water Resources Development 1991. IAEA, Vienna, pp. 33–60.
Uhlenbrook, S., Hoeg, S., 2003. Quantifying uncertainties in tracer-based hydrograph separations: a case study for two-, three- and five component hydrograph separations in a mountainous catchment. Hydrol. Process. 17, 431–453.
Walker, J.C.G., Hays, P.B., Kasting, J.F., 1981. A negative feedback mechanism for the long-term stabilization of Earth's surface temperature. J. Geophys. Res. 86, 9776–9782.
Wang, L., Zhang, L., Cai, W.J., Wang, B., Yu, Z., 2016. Consumption of atmospheric CO_2, via chemical weathering in the yellow river basin: the Qinghai-Tibet plateau is the main contributor to the high dissolved inorganic carbon in the Yellow River. Chem. Geol. 430, 34–44.
West, A.J., Bickle, M.J., Collins, R., Brasington, J., 2002. Small catchment perspective on Himalayan weathering fluxes. Geology 30, 355–358.
West, A.J., Galy, A., Bickle, M., 2005. Tectonic and climatic controls on silicate weathering. Earth Planet. Sci. Lett. 235, 211–228.
White, A.F., Blum, A.E., 1995. Effects of climate on chemical weathering in watersheds. Geochim. Cosmochim. Acta 59, 1729–1747.
White, A.F., Blum, A.E., Bullen, T.D., Vivit, D.V., Schulz, M., Fitzpatrick, J., 1999. The effect of temperature on experimental and natural chemical weathering rates of granitoid rocks. Geochim. Cosmochim. Acta 63, 3277–3291.
Williams, M.W., Melack, J.M., 1991. Solute chemistry of snowmelt and runoff in an alpine basin, Sierra Nevada. Water Resour. Res. 27, 1575–1588.
Wu, W., 2016. Hydrochemistry of inland rivers in the north Tibetan Plateau: Constraints and weathering rate estimation. Sci. Total Environ. 541, 468–482.
Wu, L., Huh, Y., Qin, J., Du, G., van Der Lee, S., 2005. Chemical weathering in the Upper Huang He (Yellow River) draining the eastern Qinghai-Tibet Plateau. Geochim. Cosmochim. Acta 69, 279–5294.
Wu, W., Xu, S., Yang, J., Yin, H., 2008. Silicate weathering and CO_2 consumption deduced from the seven Chinese rivers originating in the Qinghai-Tibet Plateau. Chem. Geol. 249, 307–320.
Wu, Y.H., Li, W., Zhou, J., Cao, Y., 2013. Temperature and precipitation variations at two meteorological stations on eastern slope of Gongga Mountain, SW China in the past two decades. J. Mt. Sci. 10 (3), 370–377.
Xu, Z., Liu, C.-Q., 2010. Water geochemistry of the Xijiang basin rivers, South China: chemical weathering and CO_2 consumption. Appl. Geochem. 25 (10), 1603–1614.
Xu, J., Zhang, W., Zheng, Z., Chen, J., Jiao, H., 2012. Establishment of a hybrid rainfall-runoff model for use in the Noah LSM. Acta. Meteor. Sin. 26 (1), 85–92.
Yang, Z.-L., Niu, G.-Y., Mitchell, K.E., Chen, F., Ek, M.B., Barlage, M., Manning, K., Niyogi, D., Tewari, M., Xia, Y.-L., 2011. The community Noah land surface model with multiparameterization options (Noah-MP): 2. Evaluation over global river basins. J. Geophys. Res. 116, D12110.
Yoon, J., Huh, Y., Lee, I., Moon, S., Noh, H., Qin, J., 2008. Weathering processes in the Min Jiang: major elements, $^{87}Sr/^{86}Sr$, $\delta^{34}SSO_4$, and $\delta^{18}OSO_4$. Aquat. Geochem. 14, 147–170.
Zakharova, E.A., Pokrovsky, O.S., Dupré, B., Gaillardet, J., Efimova, L.E., 2007. Chemical weathering of silicate rocks in Karelia region and Kola peninsula, NW Russia: assessing the effect of rock composition, wetlands and vegetation. Chem. Geol. 242, 255–277.
Zhang, Y., Hirabayashi, Y., Liu, S., 2012. Catchment-scale reconstruction of glacier mass balance using observations and global climate data: case study of the Hailuogou catchment, South-eastern Tibetan Plateau. J. Hydrol. 444–445 (10), 146–160.
Zhou, J., Wu, J., Liu, S., Zeng, G., Jia, Q., Wang, X., Zhao, Q., 2015. Hydrograph separation in the headwaters of the Shule River Basin: combining water chemistry and stable isotopes. Adv. Meteorol. 2015 (2), 1–10.
Zhou, J., Bing, H., Wu, Y., Yang, Z., Wang, J., Sun, H., Luo, J., Liang, J., 2016. Rapid weathering processes of a 120-year-old chronosequence in the Hailuogou Glacier foreland, Mt. Gongga, SW China. Geoderma 267, 78–91.